OPTICAL NANOPARTICLE FILTERING BY USING RADIATION FORCES

A Thesis Submitted to
the Graduate School of Engineering and Sciences of
İzmir Institute of Technology
in Partial Fulfillment of the Requirements for the Degree of

MASTER OF SCIENCE

in Electronics and Communication Engineering

by
Şeyma ARSLANYÜREK

December 2018
İZMİR

We approve the thesis of **Şeyma ARSLANYÜREK**

Examining Committee Members:

Prof. Dr. M. SALİH DİNLEYİCİ
Department of Electrical and Electronics Engineering
İzmir Institute of Technology

Prof. Dr. Serdar ÖZÇELİK
Department of Chemistry
İzmir Institute of Technology

Assist. Prof. Dr. Aziz KOLKIRAN
Department of Engineering Sciences
İzmir Katip Çelebi University

18 December 2018

Prof. Dr. M. Salih DİNLEYİCİ
Supervisor, Department of Electrical and Electronics Engineering
İzmir Institute of Technology

Prof. Dr. Enver TATLICIOĞLU
Head of the Department of
Electrical and Electronics Engineering

Prof. Dr. Aysun SOFUOĞLU
Dean of the Graduate School of
Engineering and Sciences

ACKNOWLEDGMENTS

First of all, I am grateful to my advisor Prof. Dr. M. Salih DİNLEYİCİ for his understanding, support, guidance in every stage of my master education.

I would like to thank Prof. Dr. Serdar ÖZÇELİK and Özge TÜCEL for their information and support.

I would like to express my gratitude to Asist. Prof. Aziz KOLKIRAN and Baha CANGÖREN for sharing their laboratory, equipment and experiences.

Finally, I would like to express my endless gratitude to my mother Hatice ARSLANYÜREK and my father Hasan ARSLANYÜREK for their support in every moment of my life.

ABSTRACT

OPTICAL NANOPARTICLE FILTERING BY USING RADIATION FORCES

In this study, it is aimed to filter nano-sized particles using light radiation pressure explicitly scattering and gradient forces. The light wave exerts momentum when encounters to the particles inside a solution. This momentum provides pulling force towards the high-intensity point as a result of gradient force and thrust in the direction of propagation resulting from scattering force. By controlling these two forces, the particles which have dissimilar properties can be moved to distinct directions. In this way, we have experimentally shown that two different particles can be separated from one another.

It has been shown mathematically that separation of two particles based on size, material properties and geometry using radiation forces. Size-based particle filtration was performed with experimental studies on particles of different sizes.

A threshold dimension value was assumed between 100 nm and 200 nm so that these particles could be separated from each other, and a design has been developed such that smaller particles are attracted towards the high-intensity point of the light with gradient force effect and larger particles are thrust in the direction of light propagation with scattering force. This setup was tested for silica particles of size 87 nm, 100 nm, 120 nm, 200 nm and 340 nm. Particles smaller than this threshold value were accumulated around the high-intensity region of light, while the larger ones continued to flow in the liquid. It has been experimentally shown that the nearest 120 nm and 200 nm particles were separated from each other. This study shows that particles with a difference of 80 nm in size can be filtered using radiation forces.

Finally, blood samples were used in experimental studies. It is shown that the thrombocyte, lymphocyte and erythrocyte cells contained in the blood can be separated from each other using radiation forces.

ÖZET

RADYASYON KUVVETLERİ KULLANARAK OPTİK NANOPARÇACIK FİLTRELEMESİ

Bu çalışmada ışığın radyasyon kuvvetleri yardımı ile nano boyuttaki partiküllerin filtrelenmesi amaçlanmıştır. Işık parçacıkla etkileşim sırasında parçacığa momentum kazandırır. Bu momentum parçacıkları ışığın yoğun olduğu noktaya doğru çeken gradyant kuvvetini ve ışığın yayılma yönünde iteren saçılma kuvvetini oluşturur. Bu iki kuvveti kontrol ederek farklı özelliklere sahip iki partikülü farklı yönlerde hareket ettirerek, birbirinden ayrıştırılabileceği gösterilmiştir.

Bu method ile boyutsal bazda, malzeme özellikleri bazında ve şekilsel bazda ayrışım yapılabileceği teorik olarak gösterilmiştir. Farklı boyuttaki partiküller üzerinde yürütülen deneysel çalışmalar ile boyut bazında partikül fitrelemesi gerçekleştirilmiştir.

Parçacıkların boyutsal bazda birbirinden ayrıştırılması için 100 nm ve 200 nm boyutları arasında bir boyut eşik değer olarak kabul edilmiştir ve bu eşikten daha küçük boyutlardaki partikülleri ışığın yüksek yoğunluk bölgesine doğru çekerek tutacak, daha büyük boyuttaki partikülleri de ışığın yayılma yönünde iterek uzaklaştıracak bir tasarım geliştirilmiştir. 87 nm, 100 nm, 120 nm, 200 nm ve 340 nm boyutlarındaki silikalar üzerinde deneysel çalışmalar gerçekleştirilmiştir. Deneysel olarak, eşik boyutun altındaki silikaların gönderilen ışığın çevresinde tutulduğu, daha büyük boyutlardaki silika partiküllerin ise doğal akışlarına devam ettiği gözlemlenmiştir. Deneysel çalışmalarda boyutsal olarak birbirine en yakın 120 nm ve 200 nm boyutlarındaki partiküllerin birbirlerinden ayrıştırılması gözlemlenmiştir. Yapılan deney sonuçlarına göre aralarında 80 nm boyut farkı olan partikülleri birbirlerinden ayırmak mümkündür.

Son olarak, kan örnekleri ile deneysel çalışmalar yürütülmüştür. Işığın hücreler üzerinde oluşturduğu radyasyon kuvvetleri ile kandaki trombositlerin, lenfosit ve kırmızı kan hücrelerinden ayrıştırılabileceği gösterilmiştir.

TABLE OF CONTENTS

LIST OF FIGURES

LIST OF TABLES

LIST OF SYMBOLS

W_0 ..... Waist radius of Gaussian beam[m]
$W(z)$ ..... Width of Gaussian beam at z position [m]
$U(\boldsymbol{r})$ ..... Complex amplitude of wave
ρ ..... Radial distance in cylindrical coordinates[m]
k ..... Wavenumber[m^{-1}]
z ..... Position for Cartesian or cylindrical coordinates[m]
$R(z)$ ..... Radius of curvature for Gaussian beam at z position[m]
$\zeta(z)$ ..... Excess axial phase of a Gaussian beam at z position
λ ..... Wavelenght[m]
I ..... Optical intensity[m]
w ..... Angular frequeny[rad.s^{-1}]
μ ..... Magnetic permeability[H.m^{-1}]
E_0 ..... Initial electric field[V.m^{-1}]
H_0 ..... Initial magnetic field[A.m^{-1}]
E ..... Electric field[V.m^{-1}]
H ..... Magnetic field[A.m^{-1}]
p ..... Dipole moment [C.m]
n_1 ..... particle refractive index
n_2 ..... medium refractive index
a ..... radius of particle[m]
ϵ_0 ..... Electric permitivity of free-space[F.m^{-1}]
ϵ_1 ..... Electric permitivity of particle[F.m^{-1}]
ϵ_2 ..... Electric permitivity of medium[F.m^{-1}]
$\boldsymbol{C}_{\text{scat}}$ ..... Scattering cross section
q ..... Charge of particle
v ..... Velocity[m.s^{-1}]
c ..... Speed of light[m.s^{-1}]
R ..... Radiation force ratio
α ..... Polarizability
M ..... Magnification ratio

LIST OF ABBREVIATIONS

SEM . . . . . Scanning Electron Microscope
FITC . . . . . Fluorescein isothiocyanate
TEOS . . . . . Tetraethyl orthosilicate
APTES . . . . . (3-Aminopropyl)triethoxysilane
UW . . . . . Ultraviolet
RBC . . . . . Red blood cell

CHAPTER 1

INTRODUCTION

Light is an important source for manipulation of microscopic scale objects. This idea is first encountered in the 19th century by studies of Maxwell and Bartoli. Bartoli succeeded in defining the radiation pressure with thermodynamical experiments (Bartoli, 1884). Within a few years, Maxwell emerged from his work on electromagnetic theory and found the radiation pressure using tensions in the ether (Maxwell, 1954). These two independent studies theoretically showed that light carried a linear momentum that would allow the particles to be manipulated. The presence of the radiation pressure was experimentally demonstrated by both Lebedev (Lebedev, 1901) and by Nichols and Hull (Nichols and Hull, 1901). There was a need for a high intensity light source to enable the defined radiation pressure to be used for moving objects. In 1960, Maiman produced the first laser and his innovation provided the necessary light source for optical manipulation.

The first reported in the history, the particle manipulation using a laser beam belongs to Ashkin from Bell laboratories. Ashkin showed that particle trapping effect with radiation pressure using two-beam (Ashkin, 1970). Then, levitation trapping was performed with using two-beam (Ashkin and Dziedzic, 1971). These two studies were carried out using the scattering force of the radiation pressure and focused on the idea of keeping the particles stable using two-beam. After these studies, the experiment of trapping to small particles with single-beam using the gradient force effect of the radiation pressure was a milestone for the optical tweezers (Ashkin et al., 1986). In this study, two forces created by the radiation pressure have been used, while the scattering force provides a motion in the direction of propagation of light besides the gradient force acts to attract the particle to the high-intensity point. This pioneering work was followed by studies of many different researchers, as well as works of Ashkin and co-workers.

The use of optical trapping on biological cells did not take long after these successful studies. Wright showed by testing biological particles of 5-10 nm in size that optical forces can manipulate biological objects(Wright et al., 1990). The absence of deterioration in the structure of biological particles during this study has opened the door to the use of radiation pressure in many areas.

Until today, using radiation pressure, manipulation of dielectric materials, metals, living cells, bacteria, viruses and DNA were carried out.

In this study, it has been shown mathematically that two particles which have different size, material or shape can be separated using radiation forces. It has also been shown experimentally that two particles of different sizes can be separated from one another. For this decomposition, it has been emphasized the gradient and scattering forces are formed by the induced momentum on the particle during the interaction of the focused laser beam with the particles contained in the solution. The scattering force consists of scattered and absorbed components on surface of the particle, however, the gradient force consists of refracted components of focused light. The scattering force tends to move the particle on propagation direction of the light, while the gradient force tends to pull the particles towards high-intensity point of the light. The difference between the directions of movement of these two forces is the basis of optical filtering. It has been mathematically shown that two different particles can be separated by moving in distinct directions with forming the gradient and the scattering forces at dissimilar magnitudes and directions. An experimental setup was created in order to obtain the focused beam which required for the particle filtering determined by the mathematical simulation. The experimental setup consists of a beam focusing system for particulate filtration and an imaging system for monitoring filtration.

Experimental studies were carried out with silicas of different sizes. In these studies, the setup parameters were adjusted in order to separate between 100 nm and 200 nm sized silica spherical nanoparticles. For this setup configuration, it was observed that 87 nm, 100 nm and 120 nm particles were collected in the high-intensity region by the effect of gradient force. However, no pulling effect was observed with the impact of radiation forces in the particles of 200 nm and 340 nm sizes. In the experimental studies carried out for filtering on the basis of size, separation of silica particles with the size of the nearest 120 nm and 200 nm was performed. In this study, a difference of 80 nm between the sizes has been observed to be sufficient for filtering. Experimental studies should be carried out on particles sizes closer to each other in order to reduce the difference between the sizes sufficient for separation. However, we did not have silicas in the dimensions between 120 nm and 200 nm, so experimental studies could not be carried out for intermediate size values. For the experimental setup, gradient and scattering forces were calculated on the particles for all silica samples. The radiation force ratio($R = F_{\text{grad}}/F_{\text{scat}}$) was calculated for these samples. It was determined that for $R > 3.6$ the particles have been collected in the high-intensity region, while for $R < 3.6$ the particles have been continued the natural flow in the solution.

Finally, experimental studies were carried out on blood samples which containing

thrombocyte cells with an average size of 0.5-1 μm, lymphocytes of 7-10 μm size and red blood cells with a size of 8 μm. The experimental studies on blood samples have been shown that thrombocyte cells can be filtered from other cells using radiation forces. The thrombocyte trapping was achieved for radiation force ratio equal to 1.38 according to experimental studies. While for blood samples R = 1.38 trapping was observed, the trapping occurred for R $>$ 3.6 for silica particles. This is due to the fact that the viscosity of the ethanol solution in which silica particles are present, was quite high than blood plasma. So the particles in ethanol were observed to be in a very rapid flow but the blood cells move very slowly compared to silica particles.

CHAPTER 2

THEORETICAL BASIS OF OPTICAL TRAPPING

Light consists of energy packages called as a photon. The photon carries energy and momentum. When the photon interacts with any particle, it can transfer its momentum to the particle. This structural feature of the photon forms the basis of radiation pressure and this effect is examined in the scattering force. In addition, the intensity distribution of light transmitted to the particle causes a force on the particle. This force is examined as gradient force as the sub-branch of the radiation pressure.

The light radiation shows the electromagnetic wave characteristic with energy propagation in space. In this study, Gauss unit system was used for definitions because particles were trapped using a Gaussian laser beam. The linear polarized Gaussian beam propagate along to z direction, the complex amplitude defined as(Saleh and Teich, 2007);

$$U(\boldsymbol{r}) = A_0 \frac{W_0}{W(z)} exp\Big[\frac{\rho^2}{W^2(z)}\Big] exp\Big[- jkz - jk\frac{\rho^2}{2R(z)} + j\zeta(z)\Big] \tag{2.1}$$

where position term r expressed with distance from beam-waist center $r = (x, y, z)$, axial position z, radial position $\rho = \sqrt{x^2 + y^2}$, wave number $k = 2\pi/\lambda$ and wavelenght λ.

The intensity of light describe as $I(\boldsymbol{r}) = |U(\boldsymbol{r})|^2$ and respectively;

$$\boldsymbol{I}(\rho, z) = I_0 \Big[\frac{W_0}{W(z)}\Big]^2 exp\Big[- \frac{2\rho^2}{W^2(z)}\Big] \tag{2.2}$$

The total power for any plane in the light z-axis is calculated by integrating the intensity in the transverse plane;

$$\boldsymbol{P} = \int_0^\infty \boldsymbol{I}(\rho, z)\, 2\pi\rho\, d\rho \tag{2.3}$$

and

$$\boldsymbol{P} = \frac{1}{2} I_0 \,(\pi W_0^2) \tag{2.4}$$

with using this power expression (2.4), intensity expression (2.2) can be rewrite

$$\boldsymbol{I}(\rho, z) = I_0 \Big[\frac{W_0}{W(z)}\Big]^2 exp\Big[- \frac{2\rho^2}{W^2(z)}\Big] \tag{2.5}$$

For the paraxial Gaussian beam with complex amplitude in (2.1), electric field expression is given by(Saleh and Teich, 2007)

$$\boldsymbol{E}(\boldsymbol{r}) = E_0 \Big(- \widehat{x} + \frac{x}{z + jz_0}\widehat{z}\Big) U(\boldsymbol{r}) \tag{2.6}$$

with the following beam parameters

$$W(z) = W_0\sqrt{1 + \left(\frac{z}{z_0}\right)^2} \tag{2.7}$$

$$R(z) = z\Big[1 + \left(\frac{z_0}{z}\right)^2\Big] \tag{2.8}$$

$$\zeta(z) = \arctan\left(\frac{z}{z_0}\right) \tag{2.9}$$

$$W_0 = \sqrt{\frac{\lambda z_0}{\pi}} \tag{2.10}$$

when expression (2.6) extended using (2.7),(2.8), (2.9), (2.10)

$$\boldsymbol{E}(\boldsymbol{r}) = E_0\left(-\widehat{x} + \frac{x}{z + jz_0}\widehat{z}\right)\frac{jkW_0^2}{jkW_0^2 + 2z}\,\exp[-jkz]$$

$$.\exp\Big[-j\frac{2kz(x^2+y^2)}{(kW_0^2)^2 + (2z)^2}\Big]\,\exp\Big[\frac{(kW_0)^2\,(x^2+y^2)}{(kW_0^2)^2 + (2z)^2}\Big] \tag{2.11}$$

where first exponential expression determines phase of plane wave, second phase front curvature and third the field intensity in transverse plane.

The magnetic field expression describes with Maxwell transforms ($\nabla \times \boldsymbol{E} = -jw\mu\boldsymbol{H}$) from the electric field expression (2.6) and is given by

$$\boldsymbol{H}(\boldsymbol{r}) = -\frac{H_0}{jw\mu}\left(\frac{1}{z + jz_0}\widehat{y}\right)U(\boldsymbol{r}) \tag{2.12}$$

For a Gaussian beam in free space, E-field, H-field and intensity expressions are defined. In instantaneous flow, the electromagnetic power is governed by the Poynting vector $\boldsymbol{S} = \boldsymbol{E}\times\boldsymbol{H}$. Time average of the Poynting vector gives us the intensity expression.

$$\boldsymbol{I}(\boldsymbol{r}) \equiv \Big\langle \boldsymbol{S}(\boldsymbol{r},t)\Big\rangle_{\mathrm{T}} = \frac{1}{2}\boldsymbol{Re}[\boldsymbol{E}(\boldsymbol{r}) \times \boldsymbol{H}^*(\boldsymbol{r})] \tag{2.13}$$

and when the intensity expression is calculated for zeroth-order approximation in a paraxial Gaussian beam (Harada and Asakura, 1996)

$$\boldsymbol{I}(\boldsymbol{r}) = \frac{n_2\epsilon_0 c}{2}|\boldsymbol{E}(\boldsymbol{r})|^2 = I(\boldsymbol{r})\widehat{z}. \tag{2.14}$$

The parameters in the points where the electromagnetic wave interacts with the particle are used to calculate the force to be applied to the particle and the momentum achieved by the particle.

2.1. Light-Particle Interaction

In the case of the interaction of electromagnetic radiation with a particle, the photons forming the radiation behave in different ways. The photons can be absorbed, reflected or refracted on the particle during this behaviors photons transfer energy and momentum to the particle. These different behaviors of photons are examined as different components of radiation forces are shown in figure 2.1(Bradshaw and Andrews, 2017). The red arrows indicate that the direct forces and the yellow arrow correspond that the indirect force. The intensity distribution is shown in blue.

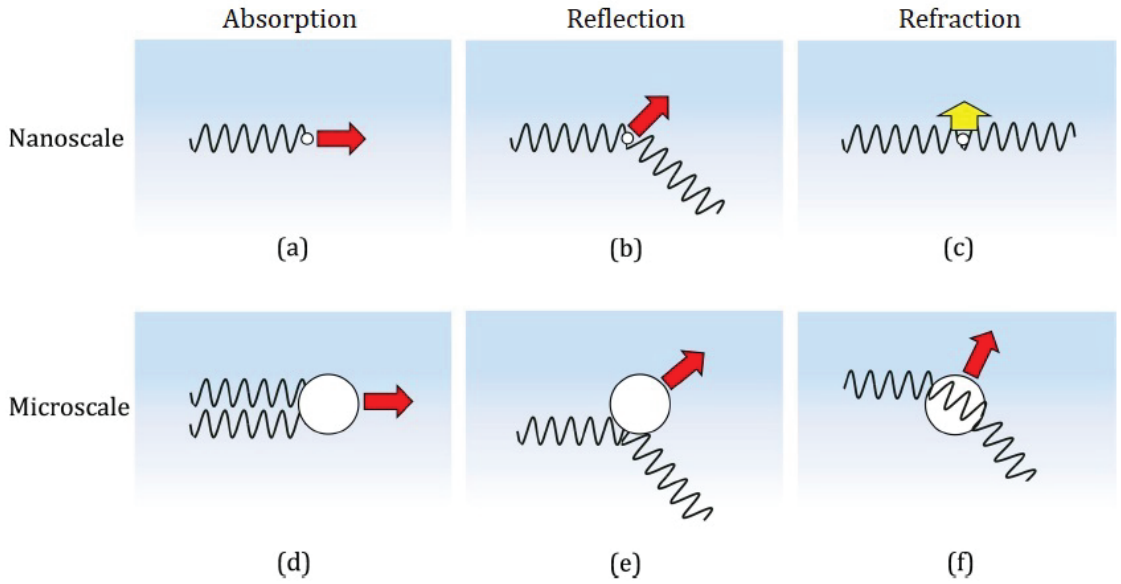

Figure 2.1. Radiation forces depend on particle size according to the behavior of the light wave

The dipole assumption can be used to define the behavior of the electromagnetic wave when the particle radius is sufficiently smaller than the wavelength of the electromagnetic wave. In this case, the spherical dielectric particle can be considered as an induced point dipole under the electromagnetic wave and the radiation pressure exerted on this dipole can have two different effects. The first of these effects is called Scattering force and forms by scattered or absorbed components of the radiation wave from the surface of the particle. The scattering force has given within Fig.2.1(a,b,d,e). The second is called Gradient force, it is formed by the effect of Lorenz force on the induced dipole and the momentum change caused by the electromagnetic wave scattered from the dipole(Svoboda and Block, 1994). The gradient force is shown with Fig.2.1(c,f).

We consider a nanoscale spherical particle with radius a, refractive index n_1, dielectric constant ϵ_1 and magnetic permeability μ_1 and this particle is standing at any point within the Gaussian beam. Beam waist center point O_{r} is assumed the center of coordinate, particle center point O_{p} and distance between these two centers r , as shown Fig. 2.2. The Gaussian beam propagates along z axis, medium refractive index n_2, dielectric constant ϵ_2 and magnetic permeability μ_2.

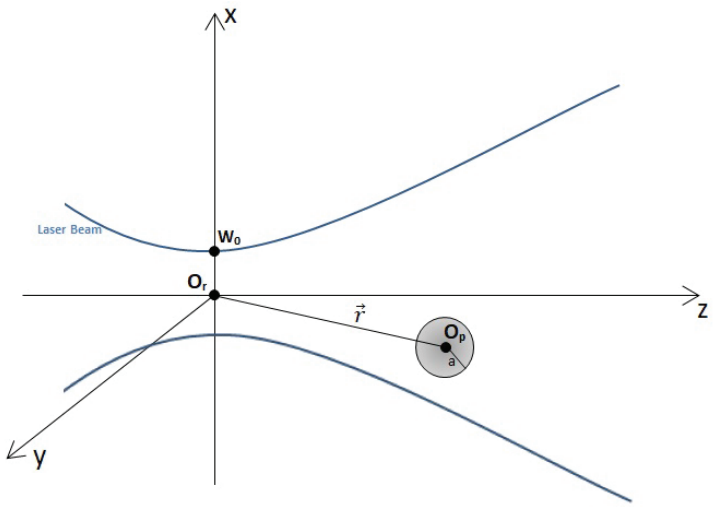

Figure 2.2. Schematic of nano-particle in a laser beam

For this defined geometry, when the size of nanosphere particle is much smaller than wavelength of the beam,it is assumed that the electric field acts equally to all points on surface of the particle and the electrostatic formulas for the dipole are applicable in this study. The electric field at surface of the particle is $\boldsymbol{E}(\boldsymbol{r},t)$ while the dipole moment on the spherical particle is given by(Stratton, 1941)

$$\boldsymbol{p}(\boldsymbol{r},t) = 4\pi\epsilon_2\, a^3\, \frac{\epsilon_1-\epsilon_2}{\epsilon_1+2\epsilon_2}\, \boldsymbol{E}(\boldsymbol{r},t)$$

$$\boldsymbol{p}(\boldsymbol{r},t) = 4\pi n_2^2\epsilon_0\, a^3\, \frac{m^2-1}{m^2+2}\, \boldsymbol{E}(\boldsymbol{r},t) \tag{2.15}$$

where m relative refractive index is rate of the particle and the medium. The spherical particle which is located in the beam, gains momentum as in (2.15) with the effect of the applied beam. When we assume that the dipole moment changes in proportion to the electric field ($\boldsymbol{p} = \alpha\, \boldsymbol{E}$) so α gives us the polarizability for spherical particle

$$\alpha = 4\pi n_2^2\epsilon_0\, a^3\, \frac{m^2-1}{m^2+2}. \tag{2.16}$$

2.2. Scattering force

The scattering force is proportional to the momentum transferred by the electromagnetic radiation to the particle during the interaction with light and particle. The light is scattered or absorbed on the particle when it encounters the particle. This scattering or absorbing events change both the magnitude and direction of the electromagnetic energy flow. During the interaction of light with matter, the particle is in a tendency to move in the direction of propagation by the momentum transferred to the beam. This effect gives us scattering force and scattering force is related with scattering cross section $\boldsymbol{C}_{\text{scat}}$ on the particle(Svoboda and Block, 1994).

$$\boldsymbol{F}_{\text{scat}}(\boldsymbol{r}) = \frac{\boldsymbol{C}_{\text{scat}} \left\langle \boldsymbol{S}(\boldsymbol{r}, t) \right\rangle_{\text{T}}}{c/n_2} \tag{2.17}$$

when rewritten the Poynting vector expression in (2.17) using (2.13);

$$\boldsymbol{F}_{\text{scat}}(\boldsymbol{r}) = \left(\frac{n_2}{c}\right) \boldsymbol{C}_{\text{scat}}\, \boldsymbol{I}(\boldsymbol{r}) \tag{2.18}$$

this indicates that the scattering force is directly proportional to the intensity and that its direction is in the direction of propagation. In this expression $\boldsymbol{C}_{\text{scat}}$ is related with geometry of the particle. For the spherical geometry given by (Kerker, 1969)

$$\boldsymbol{C}_{\text{scat}} = \frac{8}{3}\pi(ka)^4 a^2 \left(\frac{m^2-1}{m^2+2}\right)^2 \tag{2.19}$$

for this expression when (2.18) is rewritten, the scattering force expression is obtained based on the intensity.

$$\boldsymbol{F}_{\text{scat}}(\boldsymbol{r}) = \frac{8}{3}\frac{n_2}{c}\pi k^4 a^6 \left(\frac{m^2-1}{m^2+2}\right)^2 \boldsymbol{I}(\boldsymbol{r}) \tag{2.20}$$

We see from this expression that the scattering force is proportional to a^6 and is directly related to the intensity of the applied light.

The scattering force is generated by the reflected vector of the radiation applied to the particle. During this reflection, the radiated light imparts a momentum to the particle and this momentum is in the same direction with the propagation direction of the electromagnetic wave as shown in figure 2.3. Only the components of the light reflected from the particle surface are depicted in this figure. As the radius of the particle increases, the total scattering force increases as the surface area that interacts with the light increases. If the particle had a random geometry instead of spherical, the scattering on the particle

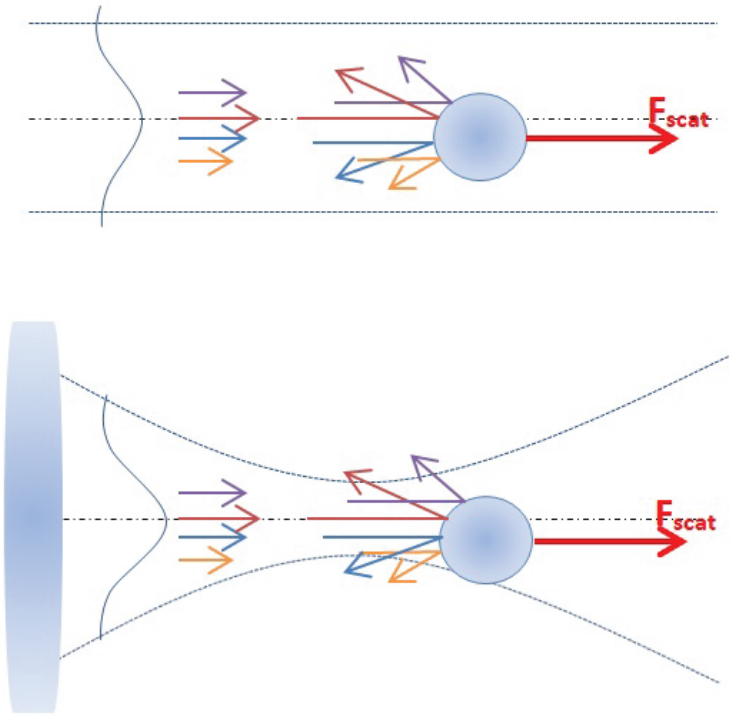

Figure 2.3. Schematic of the Scattering force (F_{scat})

surface should be observed for all points of the surface area, taking into account all scattering effects. When the particle is in a complex geometry, calculating the forces that to be exposed the particle, can become a chaotic problem.

2.3. Gradient Force

The gradient force consists of the Lorentz force induced by the electromagnetic wave on the dipole. In contrast to the scattering force, the gradient force is the product of the refracted components of light above the spherical particles. Lorentz force given by

$$\boldsymbol{F}(\boldsymbol{r},t) = q\boldsymbol{E}(\boldsymbol{r},t) + q\,\boldsymbol{v}(t) \times \boldsymbol{B}(\boldsymbol{r},t) \tag{2.21}$$

For a point dipole , distance of two charges assume as $\boldsymbol{d} = \boldsymbol{x}_1 - \boldsymbol{x}_2$ and d is infinitesimal,, the net force is calculated as $\boldsymbol{F} = \boldsymbol{F}_1 - \boldsymbol{F}_2$ and (2.21) changes as

$$\boldsymbol{F}(\boldsymbol{r},t) = q\left(\boldsymbol{E}_1(\boldsymbol{r},t) - \boldsymbol{E}_2(\boldsymbol{r},t) + \frac{d(\boldsymbol{x}_1 - \boldsymbol{x}_2)}{dt} \times \boldsymbol{B}(\boldsymbol{r},t)\right) \tag{2.22}$$

When the $\boldsymbol{E}_2(\boldsymbol{r},t)$ expression is converted according to the taylor series

$$\boldsymbol{F}(\boldsymbol{r},t) = q\Bigg(\boldsymbol{E}_1(\boldsymbol{r},t) + \big((\boldsymbol{x}_1-\boldsymbol{x}_2).\nabla\big)\boldsymbol{E}(\boldsymbol{r},t) - \boldsymbol{E}_1(\boldsymbol{r},t) + \frac{d(\boldsymbol{x}_1-\boldsymbol{x}_2)}{dt}\times\boldsymbol{B}(\boldsymbol{r},t)\Bigg) \tag{2.23}$$

and dipole moment is $\boldsymbol{p} = q\,\boldsymbol{d}$,the force takes the form

$$\boldsymbol{F}(\boldsymbol{r},t) = \big(\boldsymbol{p}(\boldsymbol{r},\boldsymbol{t}).\nabla\big)\boldsymbol{E}(\boldsymbol{r},t) + \frac{d\,\boldsymbol{p}(\boldsymbol{r},t)}{dt}\times\boldsymbol{B}(\boldsymbol{r},t) \tag{2.24}$$

we assume that the dipole moment changes in proportion to the electric field ($\boldsymbol{p} = \alpha\,\boldsymbol{E}$) so

$$\boldsymbol{F}(\boldsymbol{r},t) = \alpha\Bigg(\big(\boldsymbol{E}(\boldsymbol{r},t).\nabla\big)\boldsymbol{E}(\boldsymbol{r},t) + \frac{d\,\boldsymbol{E}(\boldsymbol{r},t)}{dt}\times\boldsymbol{B}(\boldsymbol{r},t)\Bigg) \tag{2.25}$$

The laser E-field is not change with time, so time-derivative of the electric field is zero. Finally, using Lorentz equation optained the gradient force, in its simplest form with $(\boldsymbol{E}.\nabla).\boldsymbol{E} = \nabla(1/2\boldsymbol{E}^2) - \boldsymbol{E}\times(\nabla\times\boldsymbol{E})$ and $\nabla\times\boldsymbol{E} = 0$ transformation

$$\boldsymbol{F}(\boldsymbol{r},t) = \frac{\alpha}{2}\,\nabla\boldsymbol{E}^2(\boldsymbol{r},t) \tag{2.26}$$

when the particle experience in a steady state, the gradient force obtain with time-average of Eq. (2.26)

$$\boldsymbol{F}_{\text{grad}}(\boldsymbol{r}) = \big\langle\boldsymbol{F}(\boldsymbol{r},t)\big\rangle_{\text{T}} \tag{2.27}$$

The gradient force using (2.15) and (2.26)

$$\boldsymbol{F}_{\text{grad}}(\boldsymbol{r}) = 4\pi n_2^2\epsilon_0\,a^3\left(\frac{m^2-1}{m^2+2}\right)\frac{1}{2}\,\nabla\big\langle\boldsymbol{E}^2(\boldsymbol{r},t)\big\rangle_{\text{T}} \tag{2.28}$$

where using $\big\langle\boldsymbol{E}(\boldsymbol{r},t)^2\big\rangle_{\text{T}} = \frac{1}{2}|\boldsymbol{E}(\boldsymbol{r})|^2$ transformation

$$\boldsymbol{F}_{\text{grad}}(\boldsymbol{r}) = \pi n_2^2\epsilon_0\,a^3\left(\frac{m^2-1}{m^2+2}\right)\nabla|\boldsymbol{E}(\boldsymbol{r})|^2 \tag{2.29}$$

and Eg. (2.14) is used for simplest form of gradient force

$$\boldsymbol{F}_{\text{grad}}(\boldsymbol{r}) = \frac{2\pi n_2 a^3}{c}\left(\frac{m^2-1}{m^2+2}\right)\nabla\boldsymbol{I}(\boldsymbol{r}) \tag{2.30}$$

We see from Eq. (2.30) that the gradient force is proportional to a^3.

The gradient force direction is in the same direction as the gradient of the intensity. Therefore, the particle is drawn into the high intensity region with gradient force. The direction of the gradient force changes according to the location of the particle in the beam. When gradient force is calculated in z axis from the propagation direction of light, direction and magnitude of the gradient force change is shown approximately in 2.4. Here, O_{r} is beam waist center point.

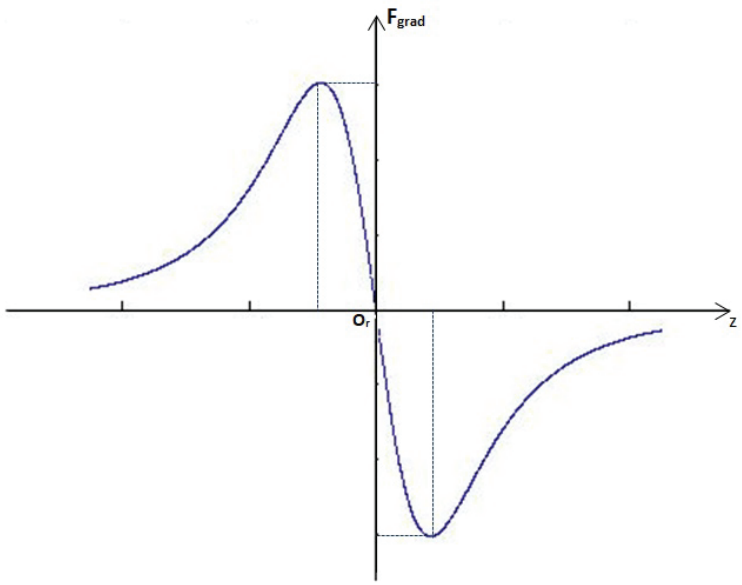

Figure 2.4. Magnitude changing of the gradient force in z-axis

The gradient force direction in the Gaussian beam is shown schematically in Fig. 2.5. The gradient force is the resultant vector of the forces $\boldsymbol{F}_{\mathrm{a}}$ and $\boldsymbol{F}_{\mathrm{b}}$ which consists of ray vectors symbolically indicated by a and b. In (2.30), the gradient force was calculated for a spherical object. For a different geometry particle and electromagnetic wave interaction, a different formulation should be formed for gradient force calculations. Because the dipole moment given in (2.15) is a definition based on geometry. Shape of the particle is important for the gradient force because it is proportional to the dipole moment and the gradient force.

2.4. Trapping Parameters

The gradient and scattering forces move the particle. The scattering force tries to push the particle towards the direction of propagation while the gradient force trying to pull the particle towards the high-intensity point. The particle remains stable at the location where these two forces eliminate each other. This location is called the trapping point. The total force on the particle

$$\boldsymbol{F}(\boldsymbol{r}) = \boldsymbol{F}_{\mathrm{scat}}(\boldsymbol{r}) + \boldsymbol{F}_{\mathrm{grad}}(\boldsymbol{r}) \tag{2.31}$$

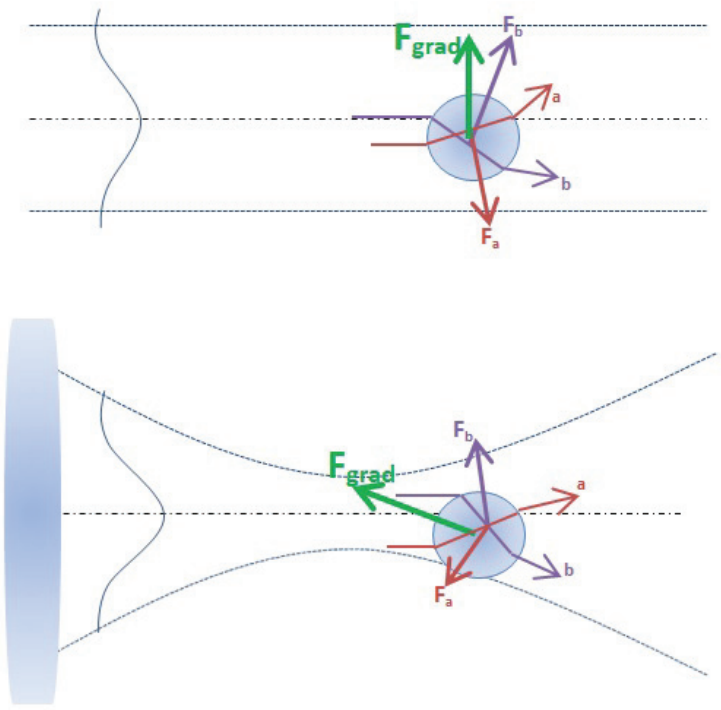

Figure 2.5. Schematic of the Gradient force (F_{grad})

varies depending on the location of the particle. The stability criterion of a single-beam trap is (Ashkin et al., 1986)

$$R = \frac{\boldsymbol{F}_{\text{grad}}}{\boldsymbol{F}_{\text{scat}}} \geq 1. \tag{2.32}$$

For the trapping of the particle, $\boldsymbol{F}_{\text{grad}}$ must be greater than $\boldsymbol{F}_{\text{scat}}$ in this case $R \geq 1$. The $\boldsymbol{F}_{\text{grad}}$ is a force with components in x, y, z axes, but $\boldsymbol{F}_{\text{scat}}$ only has the propagation direction components. The gradient force components in the x and y direction attract the particle toward the optical axis, whereas the component in the z-direction has an effect against the scattering force beyond the focus point.

The size of the particle is an important factor for trapping. The radius of the spherical particle is a and the scattering force is proportional to a^6, while the gradient force is proportional to a^3. Thus, scattering force increases faster than gradient force by increasing the size of the particle. Accordingly, trapping is easier for a small sphere than a large particle.

All the definitions so far have been made for particles present in a stagnant liquid. The gravitational force,thermal effects, the lifting force of the liquid, the drag force and the flow in the liquid were neglected. In order to keep the particle in a stable manner, these external forces must also be used in vector calculations. Drag force is the frictional

force that acts in the opposite direction of the particle in the liquid and defines as(Katz, 2010),

$$\boldsymbol{F}_{\mathrm{d}} = \frac{1}{2}\,\rho\nu^2 C_{\mathrm{D}} A \tag{2.33}$$

here, C_{D} drag coefficient which depend on shape of the particle, A cross section area, ρ density of fluid and ν velocity. Drag force is a very small force for low-viscosity, but it is the limiting effect for the minimum value of radiation forces to move the particle.

CHAPTER 3

OPTICAL FILTERING FOR NANO SCALE PARTICLES

The electromagnetic beam creates the gradient and scattering forces on small size particles and it was mentioned in previous chapters. These forces can be called as optical forces because they are formed by the focused light with optical equipment. The magnitude of the force acting on the particle change with the particle properties which interacts with the light. The forces induced by light will be different for particles with two different parameters. Therefore, the radiation forces can be customized in varied directions or in distinct magnitudes for the particles which have different parameters. As a result, the radiation forces can be used as a filter for two different particles. While one of the particles is held in the fixed position or attracted towards the focal point, the other particle is pushed forward in the direction of propagation of the light. This allows separation of the particles.

3.1. Size Based Filtering

Optical filtering by using the size difference of the particles is the filter property that gives the most obvious results. As seen in equation (2.30), the gradient force is proportional to the cube of radius of the particle, in the equation (2.20), it is seen that the scattering force is the sixth degree base of the particle size. That means the increase in particle size causes the rise on the scattering force faster than the gradient force.

Figure 3.1 shows the gradient and scattering forces for silica spherical particles with diameters of 100 nm and 200 nm. Figure (a) shows the forces acting for 100 nm and (b) for 200 nm. The horizontal axis refers to the change in z-direction on the optical axis and for $x = y = 0$. In the vertical axis, it shows the change of radiation forces to silica spherical particles. Both particles were calculated at the same distance under the same focused light. $W_0 = 5.4842\,10^{-7}$, wavelength $\lambda = 632.8$ nm, particle refractive index $n_1 = 1.4570$, ethanol which refractive index $n_2 = 1.3604$, is located on particles. 100 nm silica spherical particles can trap in stability because the F_{grad} is much greater than F_{scat}. For 200 nm, the particle cannot be captured, because the scattering force is highly effective.

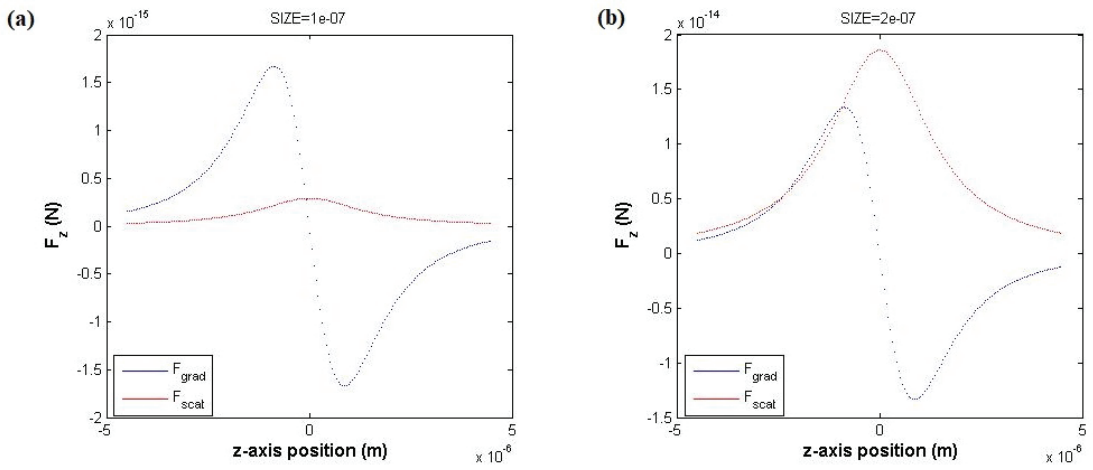

Figure 3.1. Graph of size-based radiation forces

Thus, when the same focused light is applied to two identical particles with size of 100 nm and 200 nm, they will have different effects as shown in Fig.3.2(a). The gradient and scattering forces are shown in different directions and magnitudes according to the size and location of the particle. In 3.2(b), it is shown schematically the total force acting on each particle.

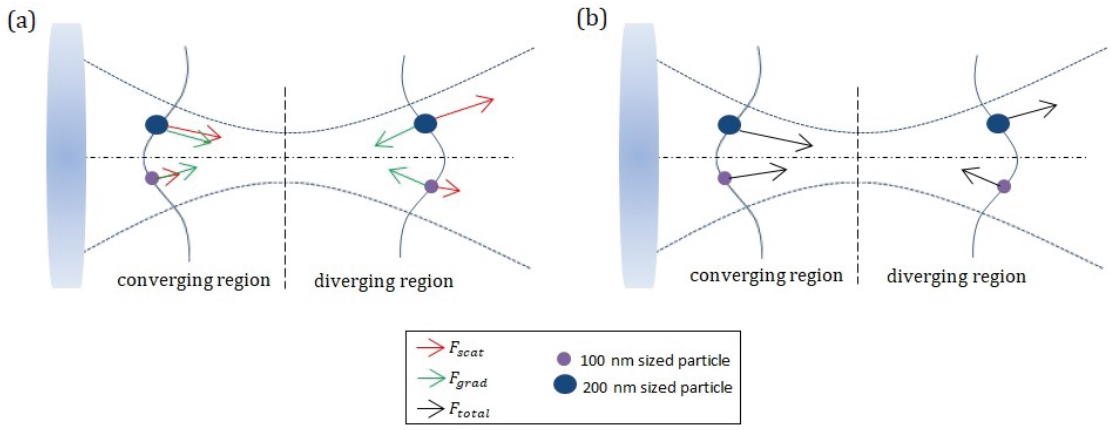

Figure 3.2. Gradient and Scattering forces and Total radiation forces for each particle

When pulling the particle size of 100 nm towards the high-intensity point, it removes the particle size of 200 nm by pushing in the propagation direction. If this process is repeated for a large number of particles, it is seen that 100 nm sized particles are collected at high-intensity region of the light and particles size of 200 nm are dragged by effect of the light and decomposition occurs.

3.2. Material Based Filtering

The rate of refractive index has a different effect on the gradient and scattering forces calculations. Therefore, different forces will act on the particles made of two different materials of the same dimensions and in the same shapes. In this way, the particles can be separated.

The optical forces calculated for silica and polystrene spherical particles with diameters of 100 nm shown in Fig. 3.3. The radiation forces are shown in Fig. 3.3.(a) for silica with refractive index $n_1 = 1.4570$ and shown in Fig. 3.3.(b) for polyester with the refractive index $n_1 = 1.5875$. The vertical axis shows the radiation forces acting on the particles and the horizontal axis shows the change in z-direction and $x = y = 0$. Both particles are in ethonel and the forces are calculated for the beam waist of propagated light as $W_0 = 1.0967\,10^{-6}$.

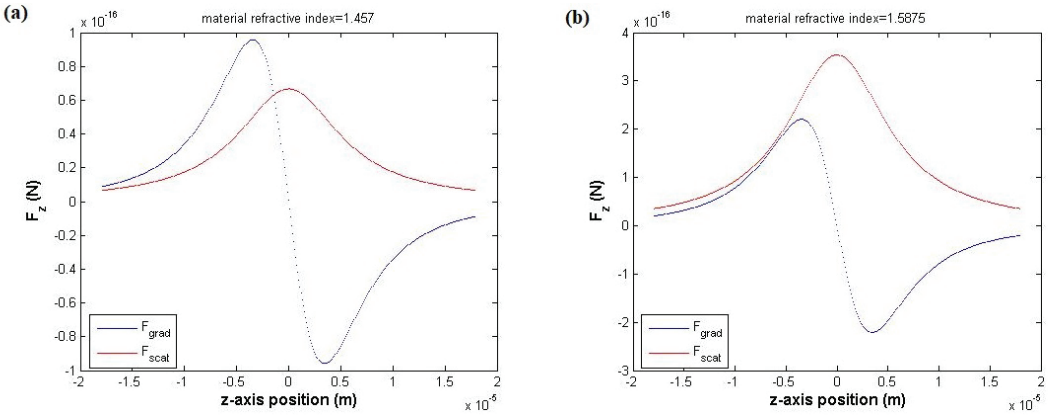

Figure 3.3. Graph of material-based radiation forces

Since the refractive index of the silica nanoparticles is smaller, the light transmittance is higher than the polyester. Therefore, the scattering force for silicas is smaller and a higher gradient force is formed. Particle capture for silica is easier than polyester. As a result, when the silica particles are collected in and around the focused light, the polyester particles are dragged away in the propagation direction of the light. Thus, particulate filtration is provided on the material-based by using the radiation forces.

3.3. Geometry Based Filtering

In order to separate the particles of different shapes, the gradient and scattering forces on the particles must be determined by taking into account the shape of the particles. The previous definitions of gradient (2.30) and scattering (2.20) forces have been given for the forces formed on spherical-shaped particles. When we rewrite the gradient and scattering force expressions in relation to polarizability(α) ;

$$\boldsymbol{F}_{\text{scat}}(\boldsymbol{r}) = \alpha\, K_{\text{s}}\, \boldsymbol{I}(\boldsymbol{r}) \tag{3.1}$$

$$\boldsymbol{F}_{\text{grad}}(\boldsymbol{r}) = \alpha\, K_{\text{g}}\, \nabla \boldsymbol{I}(\boldsymbol{r}) \tag{3.2}$$

we obtain the radiation forces independent of geometry. K_{s} and K_{g} are shape-independent coefficients for the scattering and gradient forces .

To compare the shape-based filtering, assume that the same-oriented electromagnetic field has spherical shaped (a) and cube-shaped (b) particles as in figure 3.4. The

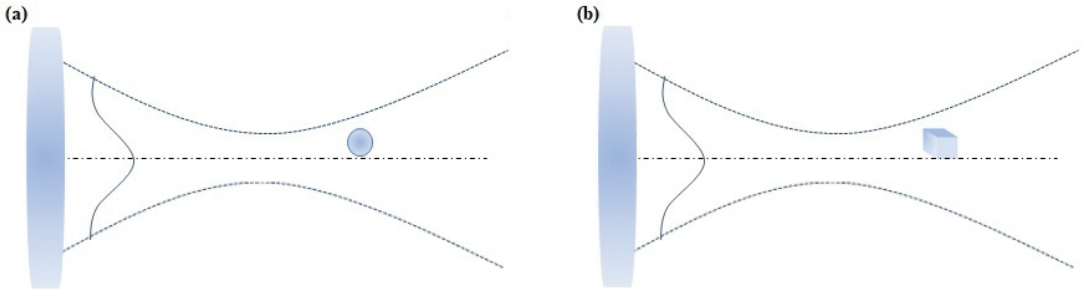

Figure 3.4. Schematic representation of geometry based filtering

dipole moment acting on the cubic shaped particles was calculated using the graph in figure 3.5(Edwards and Van Bladel, 1961). According to Fig. 3.5,the dipole moment ratios acting on spherical and cubic shaped silica particles give that the polarizability ratio for these two different geometries. For these polarizability ratios, the gradient and scattering forces on the spherical and cube shaped particles can be calculated according to the relation given in 3.1 and 3.2.

Figure 3.6 shows the radiation forces in (a) for the silica spherical particle with a diameter of 100 nm and in (b) for the silica particle in the form of a cube prism with an edge of 100 nm. It was assumed that the light in cubic prism-shaped particle came to the square plane. Accordingly, when the gradient and scattering forces are drawn on the vertical axis for focused light beam waist $W_0 = 1.2186\,10^{-6}$, it is seen that the particles

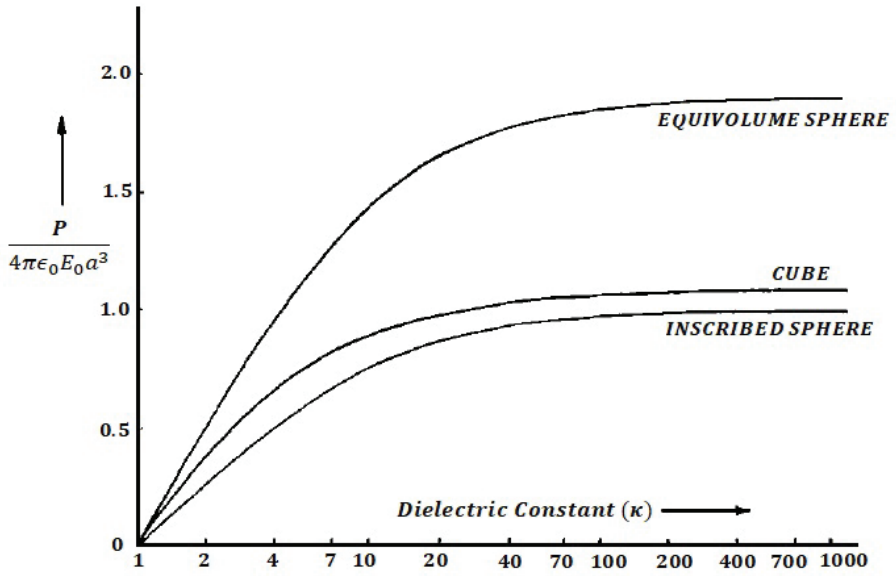

Figure 3.5. Dipole moment graph dependent on dielectric constant for cube and spherical shaped dielectric particles

will have different effects depending on the geometry. Thus, the particles can be separated according to their shape.

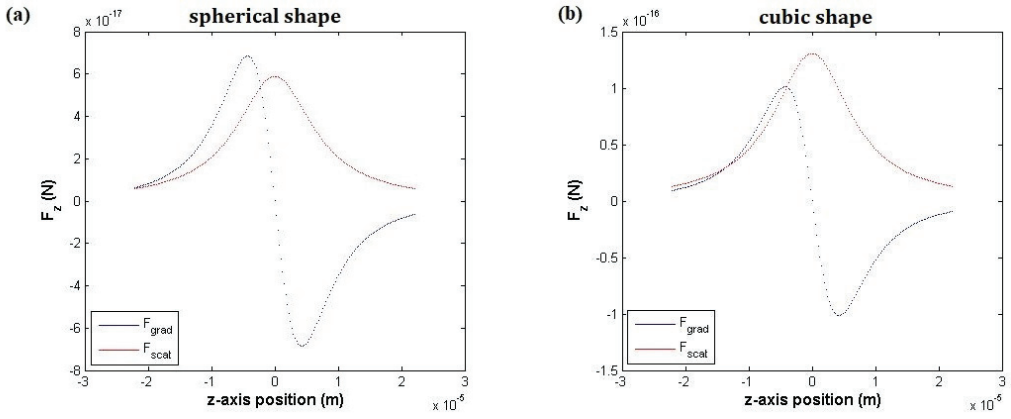

Figure 3.6. Graph of geometry-based radiation forces

We have shown here that we can decompose by calculating the radiation forces for a spherical shaped nanoparticle in figure 3.4.(a) and for a cube-shaped nanoparticle in figure 3.4.(b). Both spherical and cubic prism shapes are smooth geometric shapes that can be easily defined. Therefore, unwanted scattering effects are not observed on both of these particles. The scattering on a particle with a random geometry, the shape and surface area will be completely random. Accordingly, the effect of scattering force on

the uneven shaped object will increase. Therefore, it is difficult to calculate the forces on particles with random shapes.

CHAPTER 4

NANO-PARTICLE SYNTHESIS

The experimental studies with the particles of different sizes were carried out to examine the separation of particles with the effect of optical forces. Silica was used for syntheses to be prepared for the experimental studies. The work was carried out on the particles which refractive indexes are almost equal, spherical, silica-based, approximately 2 times difference between sizes. The colorless silica particles and APTS-FITC stained silica particle syntheses were prepared in order to observe the size-based particle filtration.

There are two different synthesis methods for obtaining silica nanoparticles, the first one is the reverse microemulsion (Yamauchi et al., 1989), the second is the Stöber method (Stöber et al., 1968). These two methods have different limitations on the adjustment and stabilization of particle sizes and in terms of synthesis time and ease of processing. In the prepared syntheses, the dimensions of the particles were adjusted with the ammonia, ethanol and TEOS ratios used during the synthesis (Durgun et al., 2011). The silica syntheses we used in the experiment were prepared by Stöber method.

The colorless silica spherical particles of 200 nm and 220 nm dimensions were prepared with the proportions of chemicals given in table 4.1. The oversized particles were obtained with an excess amount of ammonium. The colored silica nanoparticles were produced with FITC-APTES conjugate. The colored silica nanoparticles were obtained in 87 nm and 120 nm dimensions, because of their sizes smaller than colorless silicas, less amount of ammonium was used in particle synthesis.

Table 4.1. The chemical content of some silica syntheses used in the experimental studies

Dimension	ammonia		ethanol		TEOS		APTS-FITC
(nm)	(M)	(ml)	(M)	(ml)	(M)	(ml)	(ml)
200	1.14	4	0.5	30	0.14	1.2	—
220	0.91	5	0.5	30	0.14	1.2	—
87	0.016	1.5	0.5	30	0.16	1.2	0.1
120	0.012	2	0.5	30	0.16	1.2	0.1

During the synthesis, the TEOS and ethanol ratios were kept constant because the different proportions of the chemicals would have the effect of changing the density and chemical structure of the solution. Different proportions of ammonium used to adjust the dimensions caused different ph levels to be observed in the syntheses obtained. FITCH silica syntheses were about 11 ph, but the colorless silica syntheses were more basic than they were contained more NH_3. Since the colorless and colorful silicas will be used for the size-based filtering, they should not degenerate each other with acid-base imbalance when mixed with each other. Therefore after preparation the syntheses were purified and the excess ammonia and dye removed.

Dimensional distributions of colorless and FITC colored nanoparticles synthesized for use in the experiment were shown in Figure 4.1. In (a) an average of 200 nm synthesized with 4 ml of ammonium and in (b) approximately 220 nm synthesized with 5 ml of ammonium are given dimensional distributions synthesized of SINP particles.(c) is a dimensional distribution graph of FITCH SINP particles of sizes of about 87 nm prepared with 1.5 ml of ammonium and of 120 nm of FITCH synthesized with 2 ml of ammonium in (d).

The size distribution graphs show that particles were predominantly produced at certain sizes. However, the particles in small amounts were exactly dispersed inside solution except for the dimensional tolerance of 20 nm. When filtering on a size-based, calculations should be made for the size value to be decomposed considering these tolerance values.

SEM images of the particles synthesized in synthesis results to obtain spherical silica nanoparticles of 100 nm and 200 nm diameter are given in figure 4.2. Size of the synthesized silicas varies within the tolerance values. These differences in size within tolerances are seen in SEM images.

The particles were in nanoscale size and were difficult to observe the dimensional differences during imaging and to detect separation. So the particle filtration has been aimed to observe by the colors emitted from the particles during the interaction with the light. Therefore, FITC stained silicas were synthesized in the yellow color range when interacted with the UW light. It was aimed to mix the colored silicas with colored silicas and to detect the decomposition from the colors and the change in color intensity. However, as it will be explained in chapter 5, the dichroic filters which transmission graphs given in figures 5.4 and 5.7 did not transmit the yellow light wavelength. So the observation using the color changes in the particles has not realized.

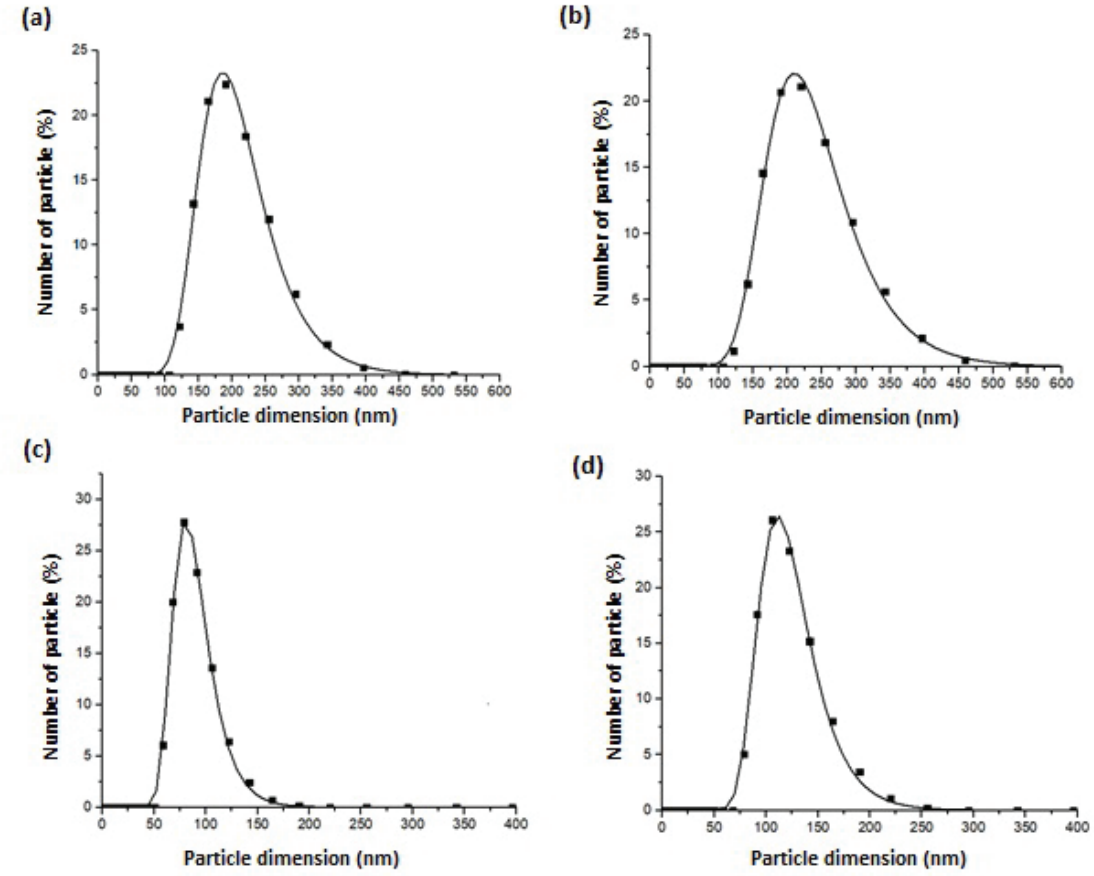

Figure 4.1. The size distributions of some synthesized nanoparticles used in the experimental studies.

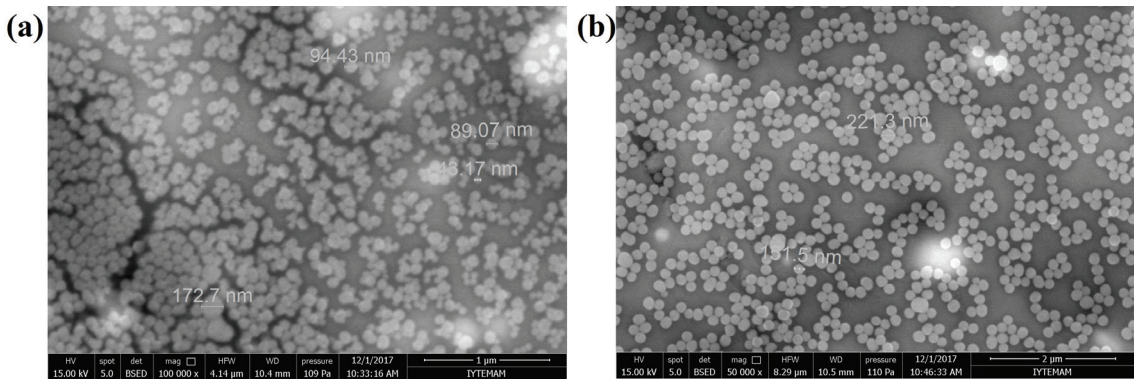

Figure 4.2. SEM images of silica spherical nanoparticles. Particle sizes approximately in (a);100nm, in (b);200nm

CHAPTER 5

EXPERIMENTAL SETUP FOR TWO PARTICLE FILTERING

To obtain a filter using radiation forces, the laser beam must be focused enough to trap the particles. A typical optical tweezer setup can be used to focus the light at the desired beam waist. Figure 5.1 shows the setup we have created for the separation of two different particles. The equipment used was selected and placed in such a way as to hold one of the particles and push the other.

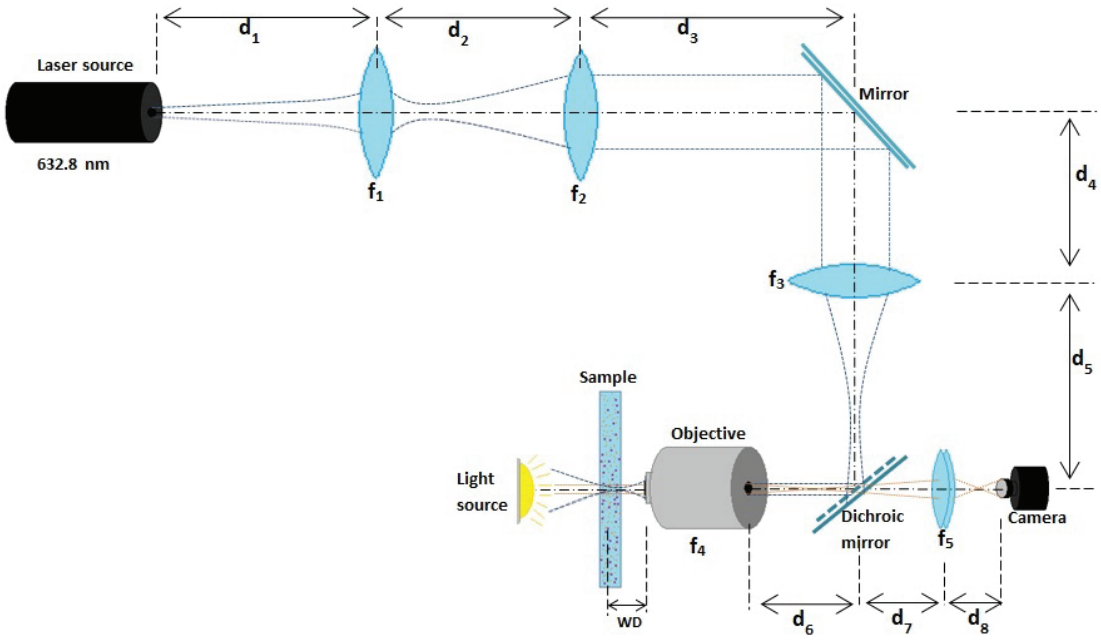

Figure 5.1. Experimental Setup

5.1. Laser Beam Focusing System

This section contains information about the experimental setup to focus the laser and filtering the particles.

5.1.1. Laser Source

In the experimental particle filtering studies, a helium-neon laser with a wavelength of 632.8 nm (red) was used as the light source. The beam diameter for this laser is 0.7 mm and the minimum output power is continuous 21mW. Since the output power of the laser to be used is proportional to the forces acting on the particles, a large amount of power is required to provide the movement of the particles.

Both the gradient and the scattering force correlate with the intensity of the applied light source. HeNe laser has generally preferred as a source in radiation forces applications because it offers low-intensity noise and good beam quality. In this application, it was used a linearly polarized source with a mode structure of more than 95 percent TEM_{00}. The use of HeNe laser has modal importance because it ensures that unstable conditions cannot occur due to other modes.

In the first installation, we used a red helium-neon laser according to the datasheet information a beam diameter of 0.8 mm and a maximum output power of 15 mW was used. However, unlike datasheet information, the output power of the laser source was measured as 6.8 mW. At the end of the arrangement in Figure 5.1, it was measured as 3.6 mW at the objective output. This power generated smaller net radiation force than the drag force. Therefore, the 6.8 mW laser output power was inadequate for particulate filtration and a stronger laser source was needed.

The power at the laser output was measured as 21.6 mW by a photodetector, when the experimental setup that is given in figure 5.1 was prepared with a laser, which has 21mW minimum output power. This power measured as 19.4 mW at f_1 lens output with 10.2% loss due to f_1 lens. The laser beam power was measured as 13.3 mW at f_3 lens output with $\%31.4$ power loss during the passage of the f_2 lens, mirror and f_3 lens. The power measured at the dichroic mirror and $100X$ objective output was 10.9 mW and $\%18$ power loss was observed. As a result of these measurements, the total power of the laser beam to manipulate the particles was measured as 10.9 mW at the objective output.

5.1.2. Lense Assembly for Trapping

The radiation forces depend on the intensity, so the magnitude of forces change with intensity characteristics of the laser. In order to separate two different particles, we must focus the laser beam for enough to trap one of the particles and push the other. For

based on size filtering, the size of 190 nm was accepted threshold, and radiation forces were calculated for this threshold value, as given figure 5.2.

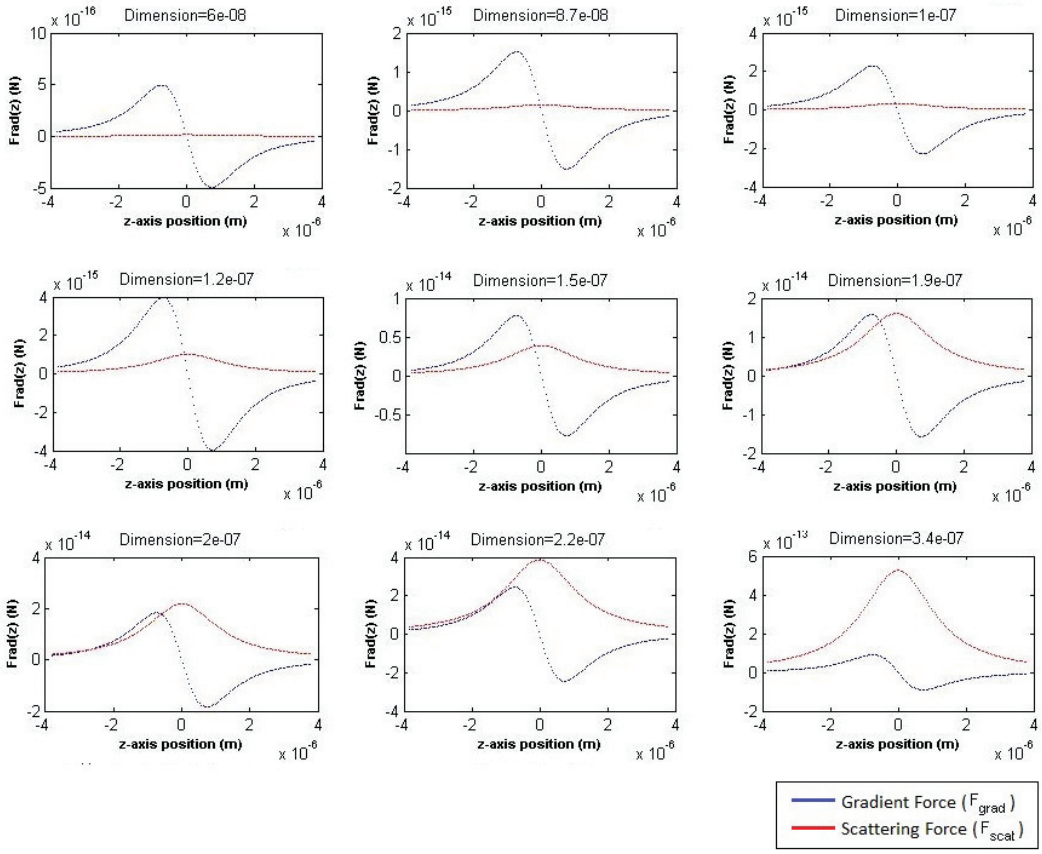

Figure 5.2. The graphs of size-based gradient and scattering forces

For particles of 60 nm, 87 nm, 100 nm, 120 nm and 150 nm in size, the gradient force is greater than the scattering force, so the particles are drawn to the focus of light. The bigger sized particles are pushed in the direction of light since the trapping condition is not met for particles of 190 nm and greater. The beam waist of the focused light that can provide this decomposition is 0.50654 μm.

In order to be able to focus light enough for the light filtering system, we have created a device as in figure 5.1. f_1 and f_2 lenses were placed at the laser output to obtain the plane wave. With the plane wave, if the position of the f_3 lens was changed, the intensity of the wave coming into the f_3 lens would remain constant. Since there is not enough space on the optical table, the plane wave was reflected with a 45° mirror to reach the f_3 lens. This mirror was also used as control equipment for change trap position on lamella. The f_3 lens was a position-adjustable lens and by changing the position of lense, we can be change the beam waist of the wave to enter the objective. By changing d_5

distance, it can be controlled the beam waist of the objective output.

In this embodiment, lenses with f_1 = 25.4 mm, f_2 = 175 mm, f_3 = 175 mm f_4 = 1.8 mm and distances with d_1=605 mm, d_2=200.4 mm, d_3=400 mm, d_4=100 mm, d_6=30 mm and d_5 adjusted as 185 mm according to calculation of mathematical model. For this setup configuration, the mathematically modeled beam waist is calculated as $0.35mm$ at the laser output, $10.58\mu m$ after f_1 lens, the waist of the plane wave at the f_2 lens output $3.3mm$, the $10.75\mu m$ after f_3 lens and $0.5654\mu m$ at the f_5 objective output. W_0 = 0.50654 μm and $z_0 = 1.27\mu m$ were obtained according to the characteristics of the beam which reached on the particles. The radiation forces were calculated for this beam as the maximum $F_{\text{grad}} = 1.57\,10^{-14}$ N and the maximum $F_{\text{scat}} = 1.60\,10^{-14}$N for size of 190nm. It was foreseen that the particles would decompose from the size of 190 nm threshold.

The mathematical calculations were made assuming that the particles were stagnant in ethanol. However, during experimental studies it has been observed that the particles are in a continuous flow because of many reasons like weight of the lamella, air flow from the outside, thermal effects, slope location of the samples, precipitation force of the particles, volatility of ethonol, and etc. In addition, during the mathematical calculation, the drag force that we had to pass in order to withdraw a particle from its own position was not taken into account.

According to calculation of the mathematical model, when the apparatus was prepared at the defined lens positions for the threshold size of 190 nm, the focused beam was not sufficient to trap the particles of size 100 nm. For separation of the particle from the size of 190 nm, we determined the distance on which light left the particles by moving the f_3 lens from the d_5 distance where the trap of 190 nm sized particles was seen. In the experimental studies, it was determined the position where the trap left the particle for the particle size of 190 nm and the distance of experimental d_5 was determined to be 220 mm. The change in d_5 distance, changes the beam waist at the objective output as given fig 5.3. In other words, by changing the position of the f_3 lens, we can control the force to be applied to the particles.

The microscope objective at a magnification of 100X was used to focus the light at maximum level. The focal length of this lens was 1.8 mm and the working distance was 0.15 mm. We used immersion oil to achieve a higher numerical aperture and a clearer image. This lens acted as the final step lens in the focusing of light in the filtering process.

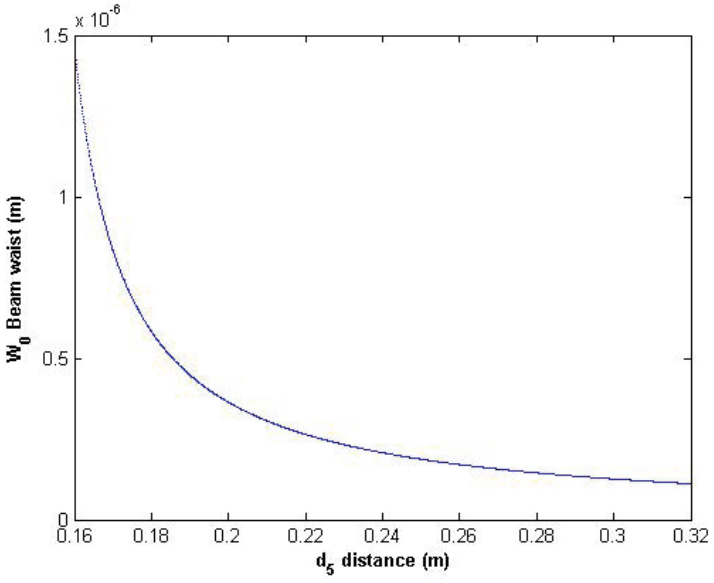

Figure 5.3. Graph of the beam waist changing with d5 distance

5.1.3. Spectral Properties of Dichroic Mirror

In the experiment setup, the wavelength-dependent dichroic mirror was used for permit both to create a path of light for particles filtering and to provide an image path to display simultaneously. The transmission rates of the dichroic mirror are given in figure 5.4. The dichroic mirror, positioned with an angle of 45° in the experimental setup, completely reflects the laser beam with the wavelength of 632.8 nm. Thus, the laser beam passes through the dichroic mirror and the objective and then reaches the particles. Besides, the illumination light used to display particles reaches the dichroic mirror through the objective lens by illuminating the particles. The dichroic mirror transmits the visible light and the image can reach the camera through the lens. The focus of light, which permits the particles to be captured and the focus of camera is within the working distance of the same objective lens. Therefore, in the same arrangement, both trapping and imaging are made possible by the use of a dichroic mirror.

5.2. Particle Imaging System

At the setup created for filtering to particles, the $100X$ objective lens was used for laser light focusing, was also used to monitor the particle traps. Optical experiments were

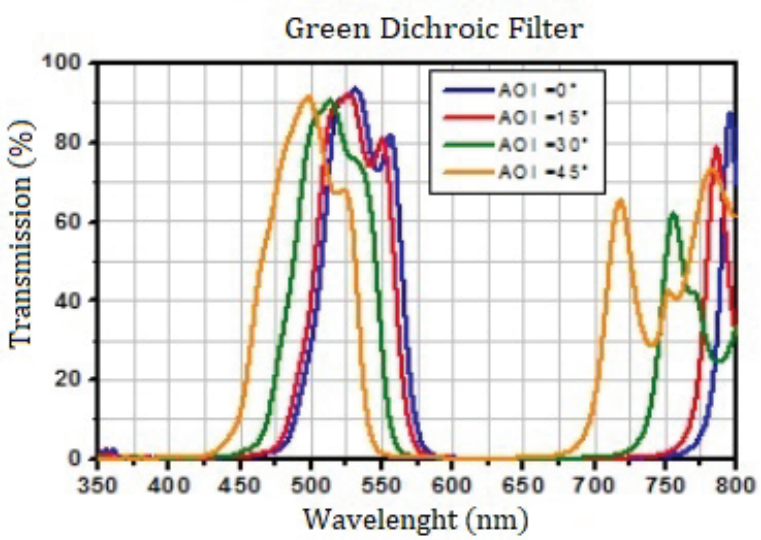

Figure 5.4. The transmission graph of the dichroic mirror

carried out on light isolating media to provide clearer imaging and to prevent unwanted glare caused from the ambient light on the lamellae and lenses. So the media was rendered dark enough. The particle imaging system setup has given in figure 5.5. An external white light was placed at the back of the samples to illuminate the particles. Images of the particles are magnified with a f_4 lens and pass through the dichroic mirror. Used dichroic mirror allows transmission in white light range. The image then reaches the camera through the f_5 lens.

In the imaging, a raspberry pi camera (raspicam) with a pixel size of $1.12\mu m \times 1.12\mu m$ and a monochromatic digital camera with a pixel size of $4.65\mu m \times 4.65\mu m$ were used. The f_5 lens was placed to increase the focal length of raspicam and to adjust the size of the image that would occur in the camera and which was removed while viewing with the other camera.

The imaging system resolution limit depends on the numerical aperture of the objective lens. In this experimental setup, an oil immersion objective lens was used. With immersion oil numerical aperture of the objective lens increased to 1.25 . When we have calculated the resolution minimum lateral dimension according to (Novotny and Hecht, 2006)

$$Min[\Delta_{\mathrm{r}}] = \frac{\lambda}{2\,\pi\,NA} \tag{5.1}$$

the resolution limit has been found as approximately 64 nm. It is possible to visualize particles greater than this resolution limit with the imaging system shown in figure 5.5.

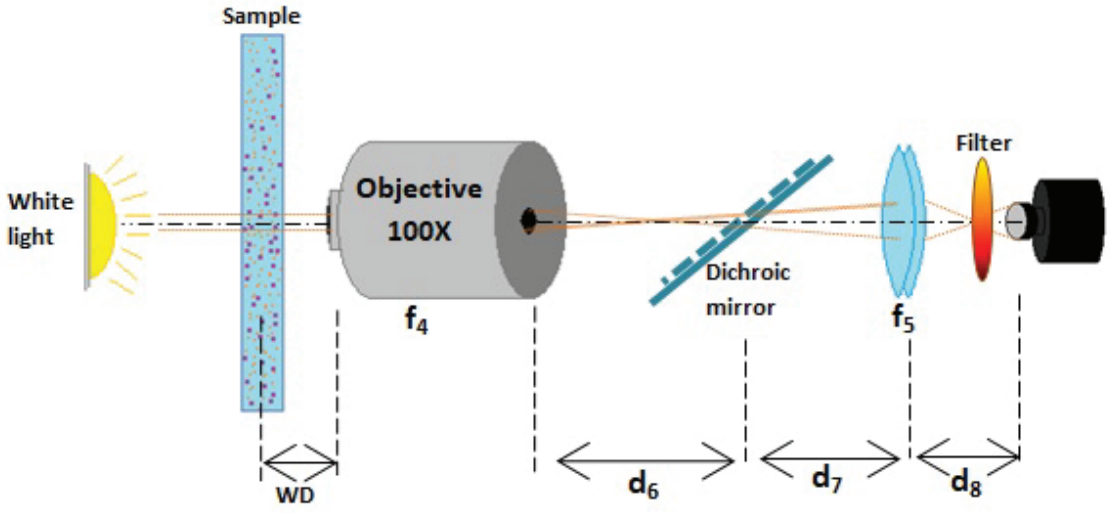

Figure 5.5. Imaging system setup

For this resolution, the image is mapped onto a distance $M\Delta_r$ in the image plane, shown with figure 5.6 .

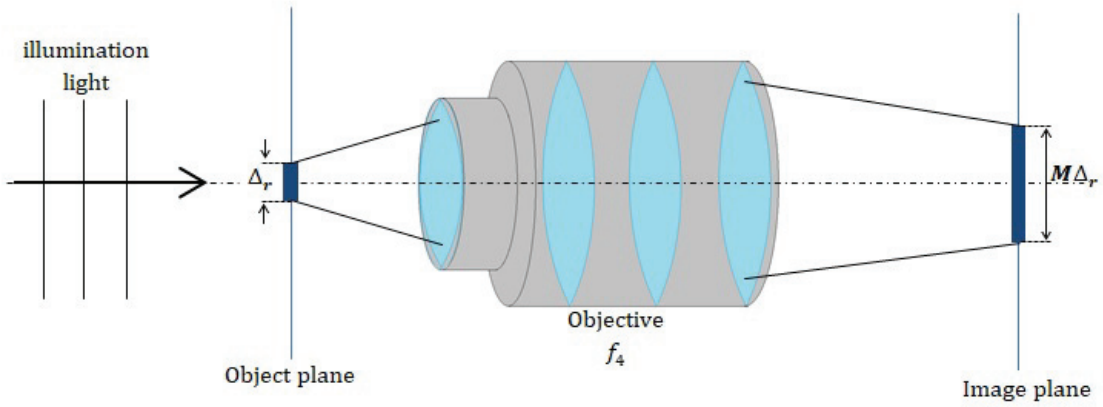

Figure 5.6. Schematic of the resolution limit

M is magnification ratio of the optical system. The magnification ratio equal to 100 for the objective lens(f_4), M increased to 150 with using f_5 lens shown as Fig. 5.5.

The dichroic mirror had to reflect all red range wavelength of the light according to the datasheet information. But during the imaging, the red light has heavily observed on the camera. So another dichroic filter has placed in front of the camera, for filtering unwanted stray light and multireflection effects. The transmission graph of the second

dichroic filter used is shown in figure 5.7.

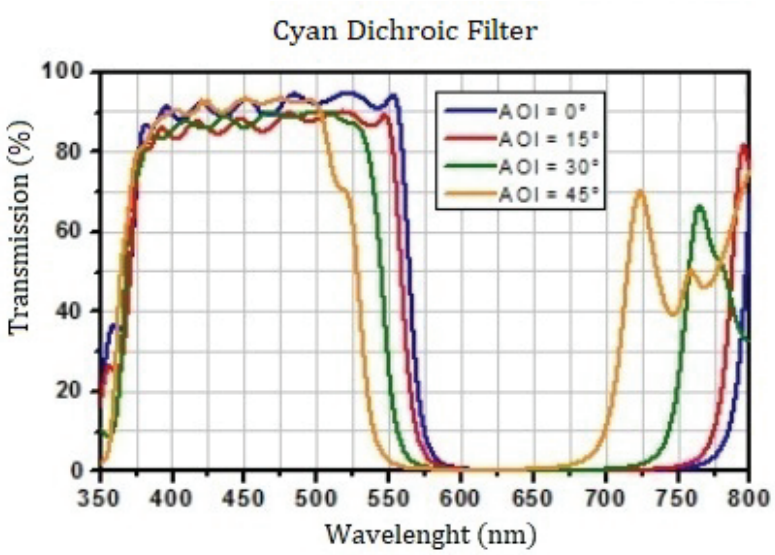

Figure 5.7. The transmission graph of the dichroic filter for unwanted stray light and multi-reflection effects

5.3. Samples for Particle Filtering

In this study, experiments were carried out on silica spherical particles size of 87 nm, 100 nm, 120 nm, 200 nm and 340 nm in order to separate the particles because of dimensional based filtration. The silica particles circulating free in ethanol were positioned at the objective output in the experimental setup by dropping between 1 mm thick glass lam and 0.13 mm thick lamella. When the particles located between lam and lamella were brought to the operating distance of the objective, manipulation of the particles with radiation forces was observed when the focal point of applied laser beam and the focal point of camera assembly were adjusted to the same plane on the samples.

In the first stage, as described in section 4, through mixed FITC-colored and colorless silicas, we envisaged observing to decomposition by the neon yellow color as a result of UW interaction with FITC. However, in Figure 5.4, the yellow light wavelength range is 560 nm - 590 nm and the transmission percentage in this range is zero. For this reason, yellow-colored radiation emitted from the interaction of FITC-colored particles with UW, which is totally reflected in the dichroic mirror and cannot reach the camera. The observation of color and colorless particles by color-based separation is not possible due to the used dichroic mirror.

We have shown that the particles can be filtered on the size-based, after adjusting the experimental setup for the 190 nm decomposition threshold. We have shown the particles filtration for all sized particles by observing the effects of the radiation forces generated by the laser focused on the particles.

CHAPTER 6

EXPERIMENTAL RESULTS AND DISCUSSION

In this chapter, for the experimental setup described in section 5, it is given the magnitude of the radiation forces acting on each particles. What kind of movement tendency of the particles against the radiation forces acting on them is indicated by the images taken with the experimental studies. The studies on silica spherical particles of different sizes were carried out on size based filtering. In the study on blood samples, separating of blood cells is given in the section of filtering on the basis of material properties.

All experimental images given in this section were taken with the monochromatic camera described in chapter 5.

6.1. Experimental Results for Size Based Filtering

Experiments were carried out for focal lenght of lenses given with f_1 = 25.4 mm, f_2 = 175 mm, f_3 = 175 mm f_4 = 1.8 mm and distances given with d_1=605 mm, d_2=200.4 mm, d_3=400 mm, d_4=100 mm, d_5=220 mm and d_6=30 mm according to the embodiment of figure 5.1. When the gradient and scattering forces for the 190 nm particles were calculated the max $F_{\text{grad}} = 21.21\,10^{-14}$ N and the max $F_{\text{scat}} = 5.88\,10^{-14}$N for determined lenses and lens positions. Although the calculated gradient force for this setup was greater than the scattering force, the net force was not sufficient to attract the particles towards the high-intensity region of the focused laser. Because there was a flow in the fluid in which the particles were contained and the net force must have overcome the drag force caused by this flow. At these configuration of lenses, the particles of 190 nm were left from the light trap. Therefore, we can think that $\boldsymbol{F}_{\text{grad}} - \boldsymbol{F}_{\text{scat}} = \boldsymbol{F}_{\text{drag}}$ for these silica samples. As the difference between the gradient force and the scattering force on the particles which smaller than the size of 190 nm is increased, the net force is greater than the drag force and the particles are captured.

The experiment was repeated on silica spherical particles of 87 nm size. The particles of 87 nm size were collected around the focused laser on the samples as shown in figure 6.1. In Fig 6.1.(a) , the laser light was given as the state before capturing any particles and the laser trap point shown in the circle. In Fig 6.1.(b) it was given after some

time focused light traps all the particles passing through the laser light. The particles were collected by attracting to high-intensity region of the focused laser with effect of the radiation forces. In Fig. 6.1, the transverse plane of the focal point of the camera is defined as the x-y axes. It was observed the collection of particles in this plane.

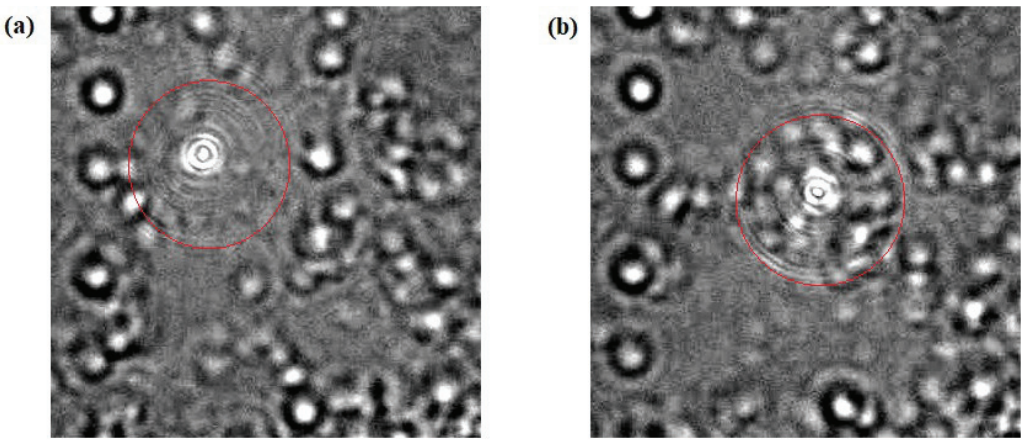

Figure 6.1. Trapping at 87 nm sized particles

For particles of 87 nm, the graphs of the radiation forces were given in figure 6.2. In Fig. 6.2(a), the changes in the x and y axes for $z = 0$, were given in terms of the x and y components of the gradient and scattering force. In Fig. 6.2(b), $x = y = 0$ was accepted and the gradient and scattering force were changed in z-axis. This was calculated as max

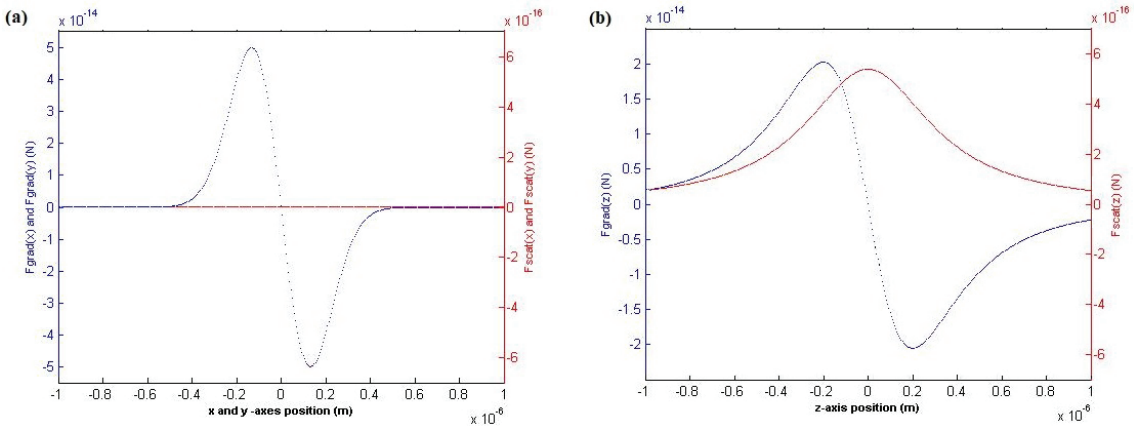

Figure 6.2. Radiation forces for the particles size of 87 nm

$F_{\text{grad}} = 2.03\,10^{-14}$ N and the max $F_{\text{scat}} = 5.42\,10^{-16}$N. The trapping force was maximum on the cross-section of the beam at a distance of $0.2\mu m$ from the center. Figure 6.3 shows schematically the magnitude of the radiation forces according to the distance from the

center of the Gaussian beam. As can be seen from both figures, the trapping area width on the transverse plane was 0.8 nm and maximum 50 particles which size of 87 nm could settle of this area. But the trap zone was not only in the transverse plane so the number of trapped particle must have been calculated in three dimensions. The Gaussian beam forms a spherical trapping area so the number of trapped particles would increase by a factor of times.

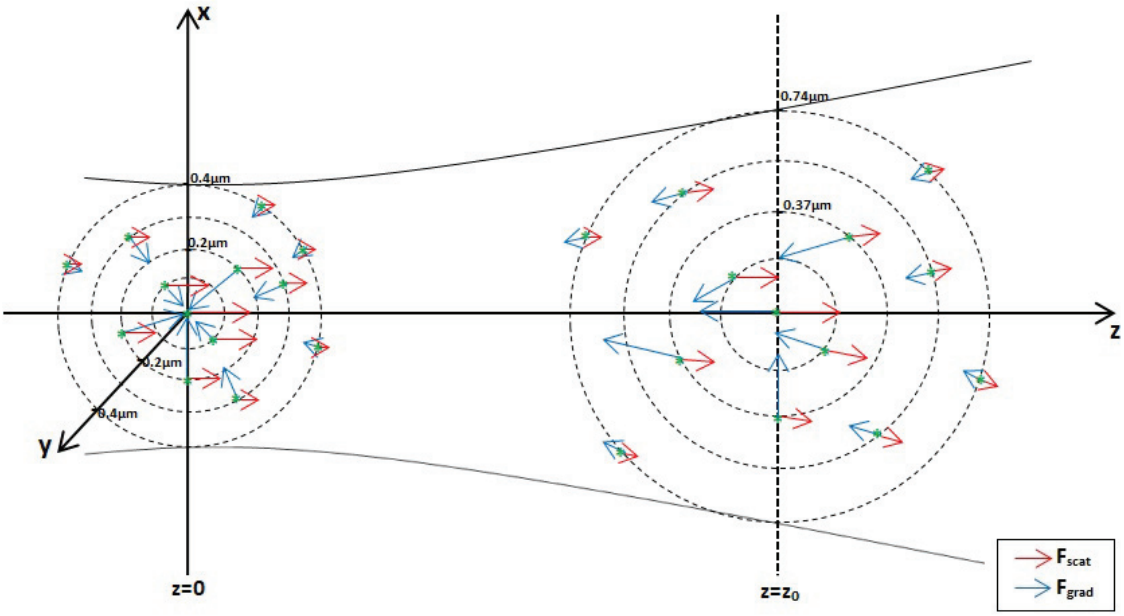

Figure 6.3. Axes-dependent representations of the radiation forces

The particle trapping was observed when the experiments were repeated for particles of 100 nm size without any modification, as in figure 6.4. The red circle shows the beam focus and the green circles indicate particles. In Fig.6.4.(a), there is no particle in the trap, but the particle pointed to green appears to approach the trap. In Fig.6.4.(b), it is shown that the impending particle is held in the trap, while the particle is in the trap, another particle shown in Fig.6.4.(c) approaches the trap. In Fig.6.4.(d) it was shown that the two particles were kept in the same trap. As it is understood from these figures, the prepared mechanism applies the force of radiation which can hold the particles of 100 nm in size. The reason we couldn't see a lot of particles in the trap, 100 nm sized particle synthesis was a more dilute mixture and there were fewer nanoparticles in ethanol. Therefore, fewer particles were retained in the trap. In a more intense sample, this number would increase.

The graph of the applied gradient and scattering forces on the 100 nm sized

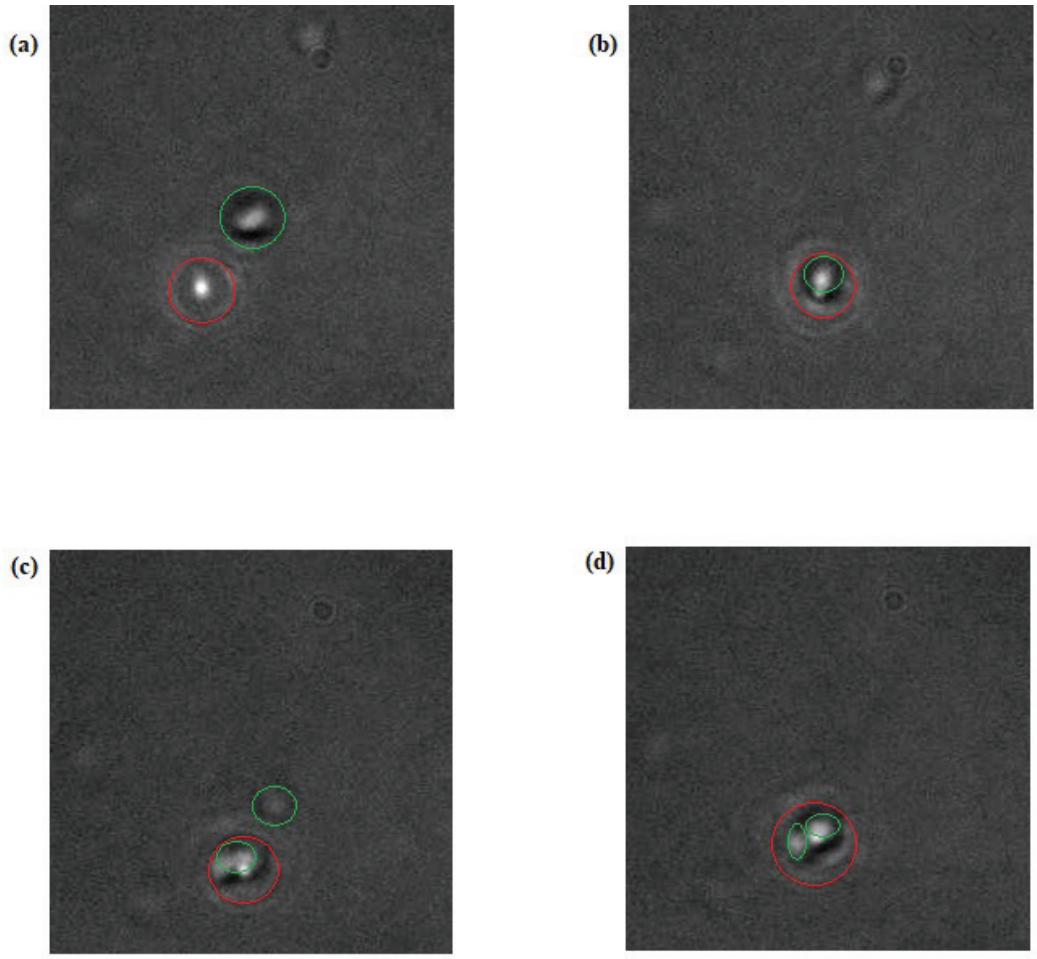

Figure 6.4. Trapping at 100 nm sized particles

particles were given in figure 6.5. The maximum $F_{\text{grad}} = 3.09\,10^{-14}$ N and the max $F_{\text{scat}} = 1.25\,10^{-15}$N on particles. The difference between the gradient force and the scattering force was sufficient to capture particles, was not as great as the difference in the 87 nm particles.

Since the setup was adjusted to hold particles up to a size of 190 nm, the focused light captured all of the silicas produced at a size of 100 nm. The size of 100 nm was the weighted ratio in the synthesis. As seen in Figure 4.1, there was 20% dimensional tolerance in all samples. Among the 100 nm syntheses, there were particles of about 120 nm in size, 5 percent. Also for these samples, the trap was realized.

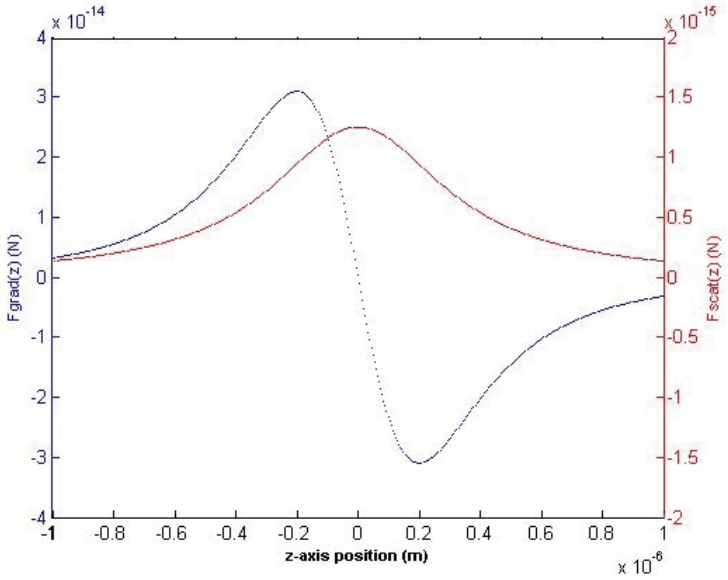

Figure 6.5. Radiation forces for the particles size of 100 nm

The same experimental setup was attempted on samples with the particles size of 120 nm without any adjustment being modified and the particle trapping observed as shown in figure 6.6. The focused light was shown in figure 6.6.(a) without any trapping and it captured a large number of particles on itself as shown in figure 6.6.(b) after a few seconds. The red circle shows the light focus in the trap area, and the green circles refer to the particles.

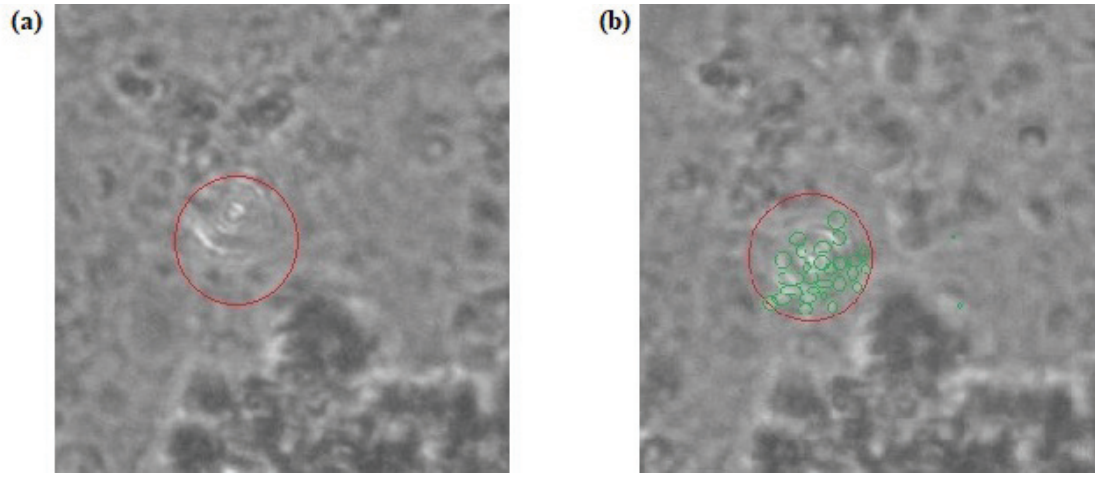

Figure 6.6. Trapping at 120 nm sized particles

The images of the particles in figure 6.6 are not as clear as in figure 6.4 and figure 6.1. This is due to the fact that 120 nm particles adhere to each other and form quite large

masses in ethanol compared to particles. Therefore, the distance between the lam and the lamella was considerably larger than in other samples. For these reasons, it was not possible during the experiments to fully focus on the objective lens for visualization of the particles.

The graphs of the calculated gradient and scattering forces for the 120 nm sized particles were given in the figure 6.7. As could be seen from the graph, the gradient force was considerably greater than the scattering force. The peak value of $F_{\text{grad}} = 5.34\,10^{-14}$ N and $F_{\text{scat}} = 3.73\,10^{-15}$N for the size of 120 nm silica spherical particles.

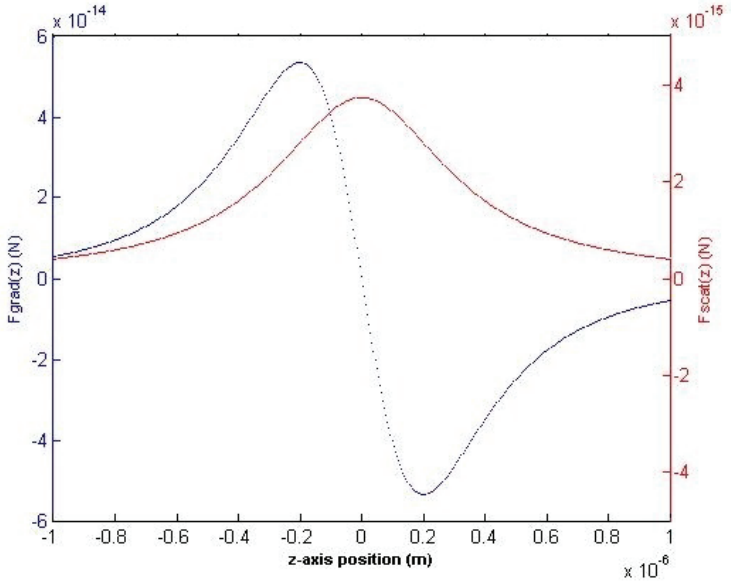

Figure 6.7. Radiation forces for the particles size of 120 nm

The gradient force for all the samples was considerably greater than the scattering force for all the examples, in all the examples given so far, the experiment was performed for dimensions smaller than the threshold size we accepted. Therefore, in all the examples we gave, the trap occurred and the light collected the particles by pulling them towards the high-intensity point.

The experimental setup was carried out on silica spherical particles of 200 nm in size without changing. But unlike the previous samples, the particles passed through the trap and continued on their way. Figure 6.8 shows the interaction of 200 nm particles with a light trap. In Fig.6.8.(a), the particle represented by the green circle approaches the light focus indicated by the red circle. In Fig.6.8.(b), it is shown the exact moment when the particle passes over the trap. In Fig.6.8.(c), it is shown that the particle continues to flow out of the trap, since the focus of light cannot provide enough force to stop the continuous

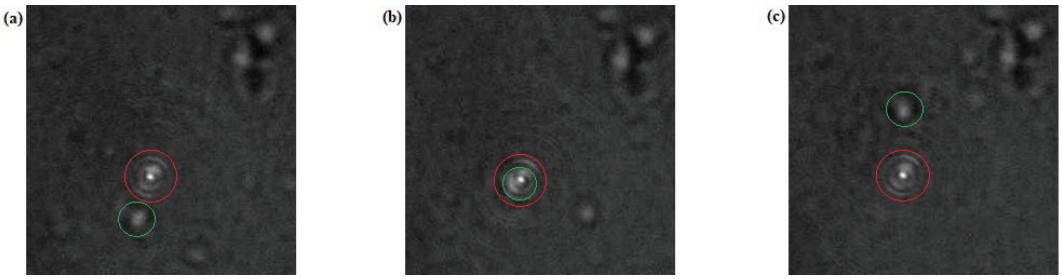

Figure 6.8. Non-trapping at 200 nm sized particles

movement of the particle and to hold the particle.

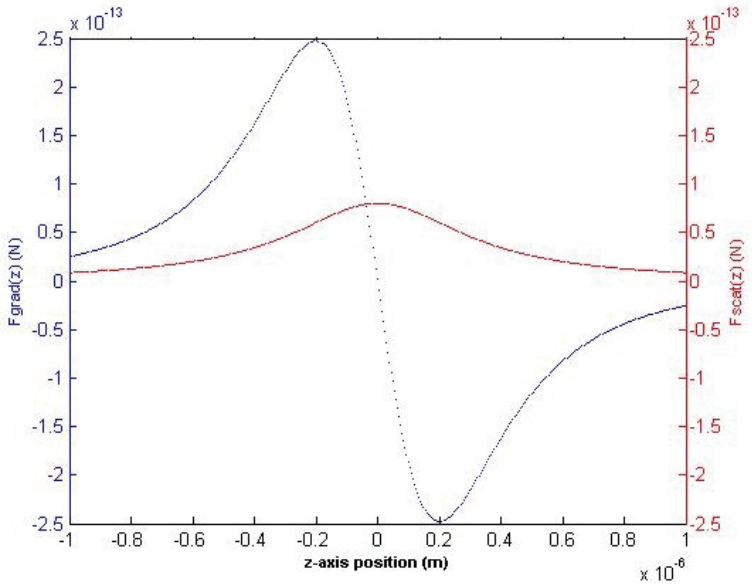

Figure 6.9. Radiation forces for the particles size of 200 nm

The radiation forces acting on particles of 200 nm were given in the graph in figure 6.9. Acting on particles with a size of 200 nm peak point of radiation forces were $F_{\text{grad}} = 2.47\,10^{-13}$ N and $F_{\text{scat}} = 8\,10^{-14}$N. The difference between gradient and scattering force was not as much as the previous examples. And the net force was not enough to pull the particles towards the high-intensity point of the light.

For the dimensional base filter application were tested on 340 nm particles, lastly. In these particles, the particle trapping with radiation forces has not been realized. In Fig. 6.10, shown particle with a green circle, in Fig. 6.10.(a) approaching to beam indicated by a red circle, in Fig. 6.10.(b) passing over the beam focal point and in Fig. 6.10.(c) moving away from the beam.

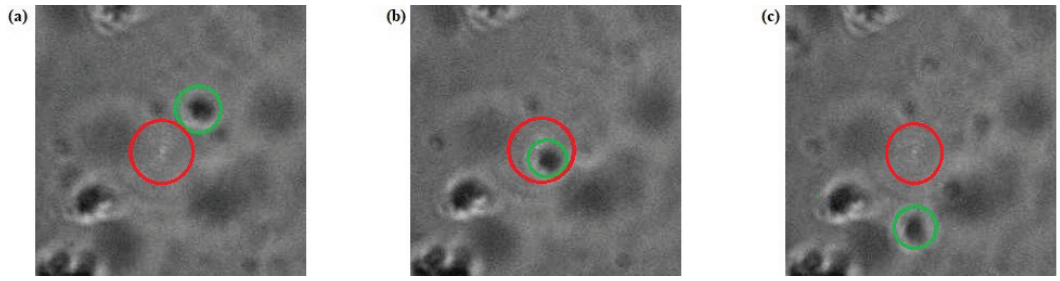

Figure 6.10. Non-trapping at 340 nm sized particles

When the radiation forces acting on the 340 nm particles are calculated, the maximum $F_{\text{grad}} = 1.21\,10^{-12}$ N and the maximum $F_{\text{scat}} = 1.93\,10^{-12}$N. As shown in figure

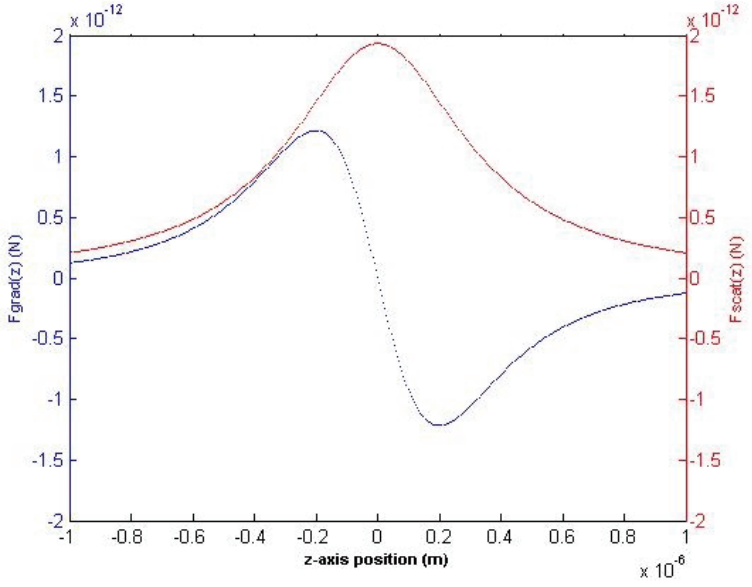

Figure 6.11. Radiation forces for the particles size of 340 nm

6.11, radiation forces generated by the intensity of focused light, which could not capture 340 nm particles even if there was no drag force on the particles. Because for 340 nm sized particles the scattering force was greater than the gradient force and the net force would drift the particle in the propagation direction of the laser beam.

The gradient and scattering forces and stability rates for all the samples we used for filtering on a dimensional basis were given in the table below. The stabiliy rate was calculated from eq. 2.32. Ideally, when the stability rate is equal to 1, the traps of the particles occur. However the stability rate should be determined depending on the density of the liquid in which the particles are contained, the particle flow velocity in the liquid,

the adhesion due to the structure of the particles, and the internal gravity forces such as cohesion. For the filtering of the particles, the forces to be applied to the particles of light must be ensured by considering the determined value of R.

In our examples, the stability criterion R was equal to 3.6 and the light above this value attracted particles towards the high-intensity region of light. Under this value could not apply any tensile force to the particles. When filtering based on size, the gradient force must have been large enough then the scattering force to the extent that the stability rate criterion would be met. For our silica-ethanol mixture samples, this ratio was determined as $R = 3.6$.

Table 6.1. Dimension-based forces and stability rate values

Dimension(nm)	F_{grad} (N)	F_{scat} (N)	$R = F_{\text{grad}}/F_{\text{scat}}$
87	$2.03\,10^{-14}$	$5.42\,10^{-16}$	37.45
100	$3.09\,10^{-14}$	$1.25\,10^{-15}$	24.72
120	$5.34\,10^{-14}$	$3.73\,10^{-15}$	14.31
190	$2.12\,10^{-13}$	$5.88\,10^{-14}$	3.60
200	$2.47\,10^{-13}$	$8.00\,10^{-14}$	3.08
340	$1.21\,10^{-12}$	$1.93\,10^{-12}$	0.63

At the beginning of this study, it was aimed to observe the effects of radiation forces on all samples synthesized in different sizes and in different colors and to mix them homogeneously and then to separate them by utilizing the radiation forces. This decomposition was intended to be observed thanks to the colors of the particles because of the detecting of the particles sizes were difficult due to their size. Therefore, as described in chapter 4, FITC stained silicas and colorless silica syntheses were performed. 87 nm FITC silicas perform a yellow glow with UW light. However, this radiation was reflected by the dichroic mirror which we had to use and cannot be observed in the camera. Without the dichroic mirror which the red color range does not refract but yellow color range passes, it is not possible to observe the targeted color change with the camera.

The Ph changes of synthesized silicas cause deterioration in the physical structure of silica. Since the chemical ratios that compose the syntheses were different from the each other, the Ph ratio of each synthesis was different from each other. When I mixed the particles of different sizes with each other, the syntheses caused changes in the chemical properties of the particles and the particles to become sticky to one another and become

useless in the experiment. In Figure 6.12, there is an image of particles deteriorated by mixing 200 nm colorless silicas with 87 nm colored silica. In this mixture, all the particles have adhered to each other. No moving particles were found in the imaging. Therefore, the dimension based filtering application experiments could not be performed on the mixed particles.

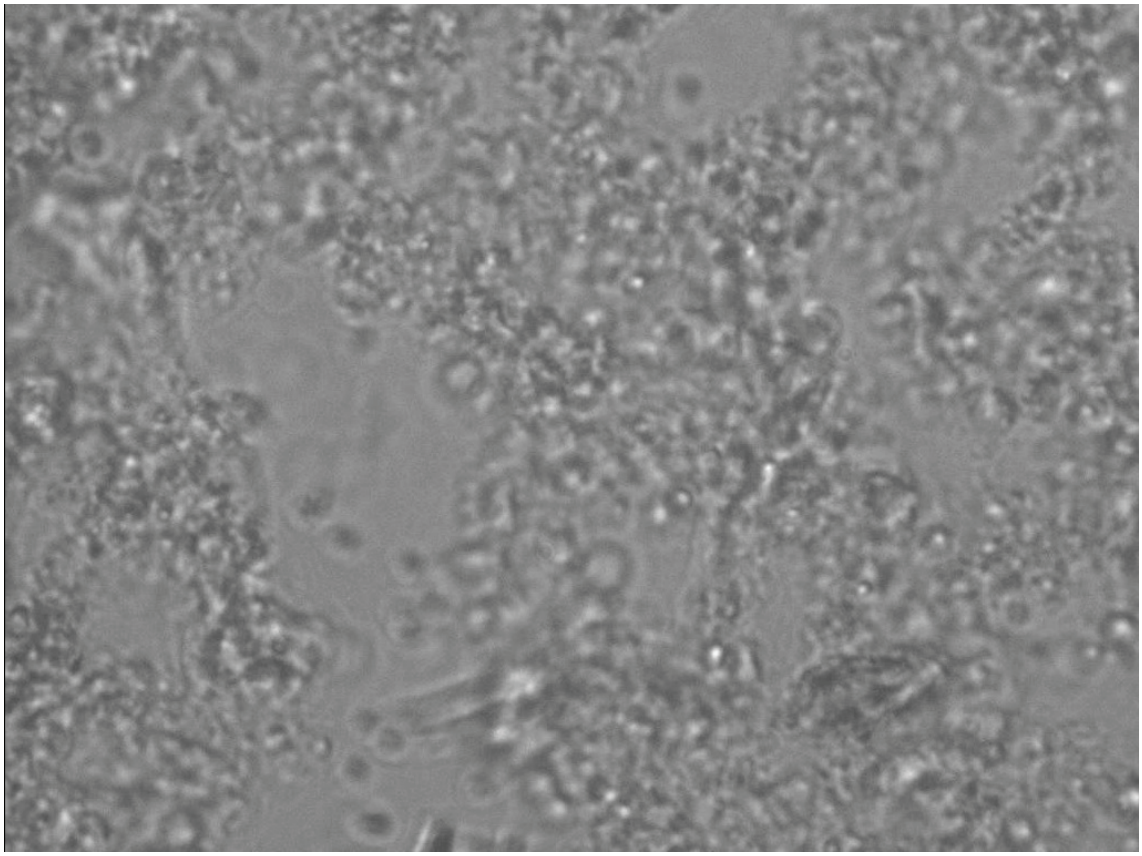

Figure 6.12. Deterioration at 87 nm FISH silica and 200 nm colorless silica mixture

6.2. Experimental Results of Material Features Based Filtering

As in figure 6.13, the blood contains platelets (thrombocyte), white blood cell (lymphocyte) and red blood cell (erythrocytes). In this study, the refractive indexes and dimensions of the cells were the main determinants for filtering using radiation forces of blood samples. Thrombocytes average sizes are 0.5-1μm and refractive index is 1.39 (Kolesnikova et al., 2006). Lymphocytes are 7-10μm and 1.35 with their dimensions and refractive index order (Keohane and W.K., Keohane and W.K.). The refractive index for

RBC is 1.4 and the average dimensions are $8\mu m$(Kinnunen et al., 2011). These cells are found in a plasma with refractive index 1.345(Bosschaart et al., 2013).

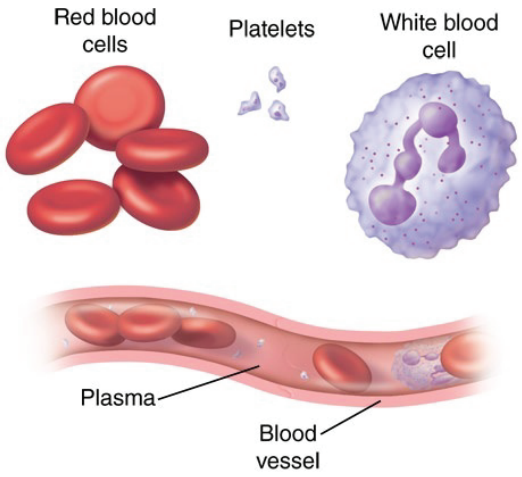

Figure 6.13. Subcomponents of blood

When we carried out experiments on blood samples with the same test setup, we could have easily separated the cells in the blood by changing the distance of d_5. The figure 6.14 shows the moment when the platelet cells were trapped. While d_5 was 280 mm, only platelets were captured from blood cells. This distance permitted the collection of the thrombocytes from the whole blood sample.

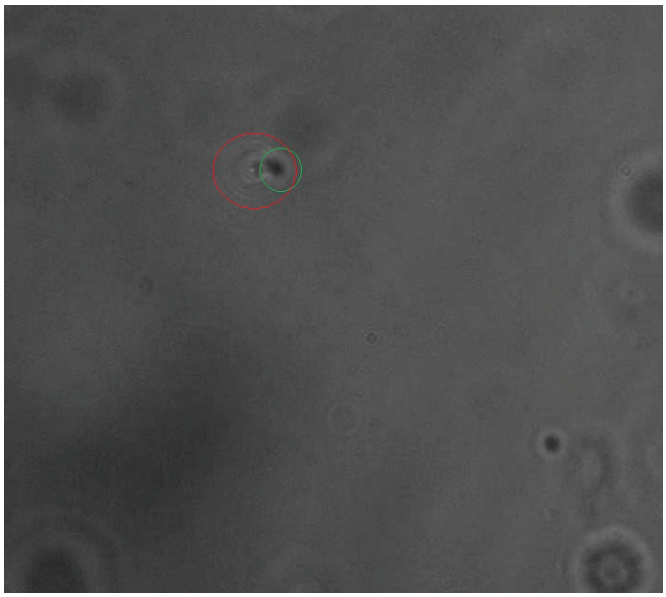

Figure 6.14. Trap of the platelet cells

Platelets cells have blood-clotting content. It should therefore be done in the case of platelets supplementation in the case that the health in the blood can be impressive when the rates are below a fixed level. Separating thrombocytes from the total blood sample is an important application for the medical field.

Figure 6.15 shows the radiation forces applied to the cells for d_5=280mm where only platelet cells were captured. In this case, the peak value of the $F_{\text{grad}} = 2.28\,10^{-11}$ N and $F_{\text{scat}} = 1.65\,10^{-11}$N. For these values, the stability rate was calculated as R = 1.38.

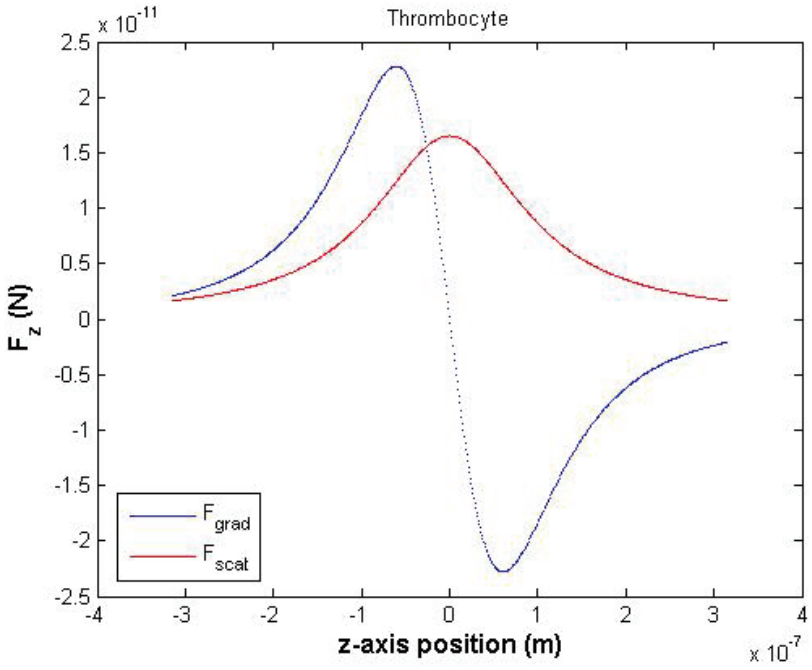

Figure 6.15. Radiation forces of the platelet cells

In R $>$ 3.6, capture was achieved in the silica samples, while for blood samples R = 1.38 capture was achieved. Because the silica particles were dimensionally smaller than the platelet cells, and because the viscosity of the ethanol was quite high than blood plasma, the particles in ethanol were observed to be in a very rapid flow. Blood samples circulate in a mixture of blood plasma and water and they appear to move very slowly compared to silica. Therefore, the difference between the gradient force and the scattering force does not need to be very large, as in the case of silica.

Figure 6.16 shows the trap side of the lymphocyte cells on the light side. The d_5 distance of the installed device was capable of applying high radiation forces for trapping to the whole blood cells.

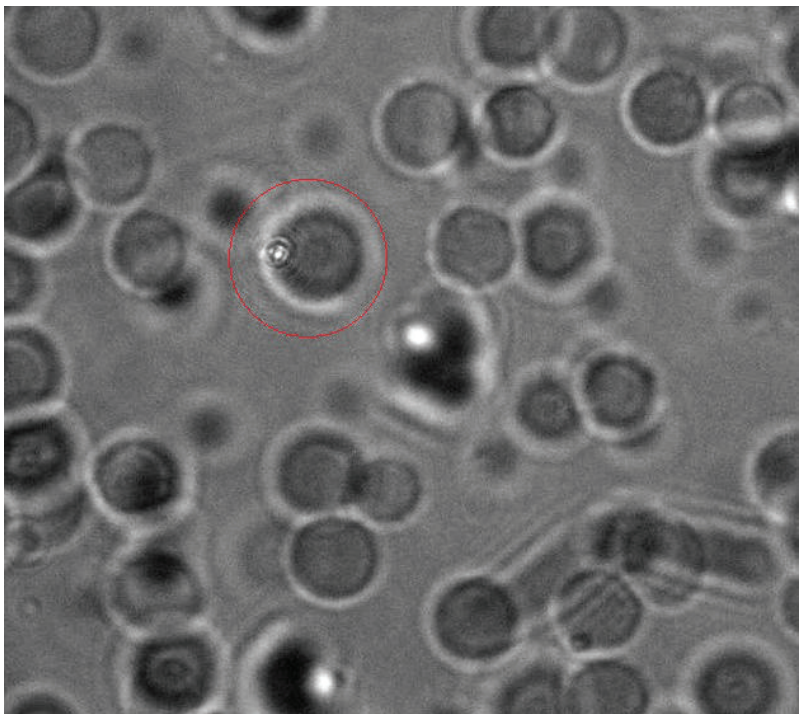

Figure 6.16. Trap of the lymphocyte cells

CHAPTER 7

CONCLUSION

This thesis aims to show that light can be used to separate the nanoparticles having different properties from each other by exploiting the radiation forces that occur during the interaction between the light and the particles. The main objective of the thesis is the nanoparticle filtering based on size, shape, and material properties. The previous studies in the literature indicate that particles can be manipulated using radiation forces. In this thesis, we have focussed that two different nanoparticles can be filtered based on size using radiation forces.

The experimental studies have been carried out on silica spherical particles of 87 nm, 100 nm, 120 nm, 190 nm, 200 nm and 340 nm. These particles are not well-separated form in ethanol solution. In these experimental studies, the radiation forces acting on the particles have various gradient and scattering forces components depending on the particle size. The gradient forces collected the 87 nm, 100 nm and 120 nm particles in the high-intensity region of the light but no collecting effect was observed at 200 nm and 340 nm sized particles. As a result, the experiments reveal that the radiation forces make possible to size-based nanoparticle filtering between two particles which have close sizes.

In the similar experiments on blood samples, the platelets have been separated from the other cells using the radiation forces thanks to size differences and refractive index differences among platelets, white blood cells and red blood cells. These experiments have shown that a optical setup can be formed that can distinguish between platelets, white blood cells and red blood cells.

In order to investigate how close two particles can be distinguished, the experimental setup has been modified by adjusting configuration of the optical components so as to obtain the beam (intensity) characteristic required for separation of the particles. This modification permitted to collect the 100 nm sized particles in the high-intensity region of the light but no trapping effect has been observed for the 200 nm sized particles. For this case, it was observed that 120 nm particles were also collected in the high-intensity region. When 190 nm sized particles were tested, no steady state was observed although it was for 200 nm sized particles. Part of the 190 nm particles were retained in the high-intensity region while some of them continued in the natural flow. Therefore the value of 190 nm size might be considered as a threshold value for this configuration. The stability

criterion of the particles that given by $R \geq 1$ in the literature indicates the trapping without the drag force effect. The experimental studies on silica nanoparticles demonstrated that for $R > 3.6$ which was calculated for the threshold value, the particles were collected in the high-intensity region of light. For $R \leq 3.6$, no trapping was observed on the particles. In the experiments on blood samples, the ratio of radiation forces was observed as $R = 1.38$ on the platelet cells. This is not stability criteria for the platelets. The experimental studies on blood samples were carried out in the optical setup configuration where platelets could be captured and separated from the other cells. To determine the stability criterion for the platelets, the minimum rate of force required for trapping of the platelets should be determined by experimental studies however we can suggest that this value is less than 1.38 .

The experimental results on silica particles and blood cells have shown that the stability criteria for two nanoparticle filtrations needs to be modified including that the fluidity of the solution. Since the viscosity is a factor that increases the drag force, reducing this force decreases the stability criterion.

According to these experimental results, the particles with 80 nm size deviation can be separated from each other. The size distribution graphs of the particles are given in figure 4.1. The silica nanoparticles have size variance within tolerance values given by approximately ± 50 nm for 200 nm sized particles and approximately ± 30 nm for 120 nm sized particles. Therefore, the dimensional fluctuations of the particles have a limiting effect in the size-based filtering .However, in order to obtain the minimum size deviation required for nanoparticle filtering, the experiments can be performed for particles which have lower size tolerance in the size range between 120 nm and 200 nm.

In this study, we have shown that we can control the radiation forces on the particles by changing the intensity distribution of the laser beam and we can perform particle filtration by using these radiation forces. This filtering can be carried out on the size-based or on the shape-based. The gradient and scattering forces on the particles that have the same size and material properties but different shapes are given in figure 3.6 according to the mathematical modeling. A differences in the geometries of the particles have various effects on the gradient and scattering forces exploited on the particle. Thanks to these effects, a setup can be developed that enables the particles to be filtered according to their shape using radiation force. The particles of the same size which are made from the same material can be separated from the malformed ones. In this way, a solution with homogeneous shape distribution can be obtained.

REFERENCES

Ashkin, A. (1970). Acceleration and trapping of particles by radiation pressure. *Phys. Rev. Lett 24*, 156.

Ashkin, A. and J. Dziedzic (1971). Optical levitation by radiation pressure. *Appl. Phys. Lett 19*, 283–285.

Ashkin, A., J. Dziedzic, L. Bjorkholm, and S. Cho (1986). Observation of a single-beam gradient force optical trap for dielectric particles. *Opt. Lett 11*, 288–290.

Bartoli, A. (1876−1884). *Il calorico raggiante e il secondo principio di termodynamica*, pp. 193–202. Nuovo Cimento.

Bosschaart, N., G. J. Edelman, M. C. G. Aalders, T. Leeuwen, and D. J. Faber (2013). A literature review and novel theoretical approach on the optical properties of whole blood. *Lasers Med Sci. 29*, 453–479.

Bradshaw, D. and D. Andrews (2017). Manipulating particles with light: radiation and gradient forces. *European Journal of Physics 38*, 034008.

Durgun, G., K. Ocakoglu, and S. Ozcelik (2011). Systematic tuning the hydrodynamic diameter of uniformed fluorescent silica nanoparticles. *Journal of Physical Chemistry 115*, 16322–16332.

Edwards, T. W. and J. Van Bladel (1961). Electrostatic dipole moment of a dielectric cube. *Applied Scientific Research 9*, 151–155.

Harada, Y. and T. Asakura (1996). Radiation forces on a dielectric sphere in the rayleigh scattering regime. *Optics Communications 124*.

Katz, J. (2010). *Introductory fluid mechanics*. Cambridge University Press.

Keohane, K. and M. W.K. The cytoplasmic refractive index of lymphocytes, its significance and its changes during active immunization.

Kerker, M. (1969). *The Scattering of Light and Other Electromagnetic Radiation* (1st ed.). Academic Press.

Kinnunen, M., A. Kauppila, and R. Myllyla (2011). Effect of the size and shape of a red blood cell on elastic light scattering properties at the single-cell level. *Biomed. Opt. Express. 2*, 1803–1814.

Kolesnikova, I., S. Potapov, M. Yurkin, V. Hoekstra, A.G. aand Maltsev, and K. Semyanov (2006). Determination of volume, shape and refractive index of individual blood platelet. *Journal of Quantitative Spectroscopy and Radiative Transfer 102*, 37–45.

Lebedev, P. (1901). Experimental examination of light pressure. *Ann. Phys. 6*(433).

Maxwell, J. (1954). *A treatise on electricity and magnetism*, Volume 2. Dover.

Nichols, E. and G. Hull (1901). A preliminary communication on the pressure of heat and light radiation. *Phys. Rev. 13*(307-20).

Novotny, L. and B. Hecht (2006). *Principles of Nano-Optics*. Cambridge University Press.

Saleh, B. E. A. and M. C. Teich (2007). *Fundamentals of Photonics* (2nd ed.). John Wiley and Sons.

Stöber, W., A. Fink, and E. Bohn (1968). Controlled growth of monodisperse silica spheres in the micron size range. *Journal of Colloid and Interface Science 26*, 62–69.

Stratton, J. A. (1941). *Electromagnetic Theory*. John Wiley and Sons.

Svoboda, K. and S. Block (1994). Biological applications of optical forces. *Annual review of biophysics and biomolecular structure 23*, 247–285.

Web, C. https://www.stanfordchildrens.org/en/topic/default?id=what-are-white-blood-cells-160-35.

Wright, W., G. Sonek, T. Tadir, and M. Berns (1990). Laser trapping in cell biology. *IEEE Journal of Quantum electronics 26*, 2148–2157.

Yamauchi, H., T. Ishikawa, and S. Kondo (1989). Surface characterization of ultramicro spherical particles of silica prepared by w/o microemulsion method. *Colloids and Surfaces 37*, 71–80.